Supplementary Information: Selective and Collective Actuation in Active Solids

P. Baconnier[1], D. Shohat[1,2], C. Hernández López[3,4], C. Coulais[5], V. Démery[1,6], G. Düring[3,4], O. Dauchot[1]

[1] *Gulliver UMR CNRS 7083, ESPCI Paris, Université PSL, 75005 Paris, France*

[2] *School of Physics and Astronomy, Tel-Aviv University, Tel Aviv 69978, Israel*

[3] *Instituto de Física, Pontificia Universidad Católica de Chile, Casilla 306, Santiago, Chile.*

[4] *ANID - Millenium Nucleus of Soft Smart Mechanical Metamaterials, Santiago, Chile.*

[5] *Van der Waals-Zeeman Institute, Institute of Physics, Universiteit van Amsterdam, Science Park 904, 1098 XH Amsterdam, the Netherlands.*

[6] *Univ Lyon, ENSL, CNRS, Laboratoire de Physique, F-69342 Lyon, France.*

Here, we provide supplementary informations including movies that illustrate our main findings, details about experimental methods and data analysis and a comprehensive description of the theoretical model outlined in the main text, which accounts for the noiseless and over-damped dynamics of self-propelled polar particles embedded in an elastic network. For the sake of clarity, this document is written in a self-consistent fashion, all the notations and definitions of the main text are explicitly re-defined. The document is organized as follow:

1 List of supplementary movies **2**

2 Model **2**
- 2.1 General equations . . . 2
- 2.2 Experimental measure of the microscopic parameters . . . 3

3 The harmonic approximation **6**
- 3.1 Formulation of the harmonic approximation using Bra-ket notations . . . 6
- 3.2 Projection on the normal modes . . . 6

4 Fixed points stability analysis **7**
- 4.1 An infinite set of fixed points . . . 7
- 4.2 Dynamics linearized around a given fixed point . . . 7
- 4.3 Properties of the spectrum valid for all fixed points . . . 7
- 4.4 Stability threshold of a given fixed point . . . 8
- 4.5 First linear destabilization . . . 8
- 4.6 Upper bound of the stability thresholds . . . 9

5 One particle dynamics **10**
- 5.1 Governing ODEs . . . 10
- 5.2 Fixed Points . . . 10
- 5.3 Orbiting solutions in the degenerate case . . . 11
- 5.4 Influence of the bias . . . 11

6 Coarse-grained model **12**
- 6.1 Continuous fields . . . 12
- 6.2 Strain dynamics . . . 12
- 6.3 Polarity dynamics . . . 13
- 6.4 Final form with polarization relaxation . . . 14
- 6.5 Disordered phase . . . 14
- 6.6 Homogeneous phases . . . 15

7 N particles dynamics : symmetry considerations **16**
- 7.1 Normal modes sorted by class of symmetry in D_6 geometry . . . 16
- 7.2 Normal modes sorted by class of symmetry in D_2 geometry . . . 17
- 7.3 Symmetry constraint on the mode selection. . . . 17

8 N particles dynamics restricted to two modes **17**

9 Dynamics of linear structures **19**
- 9.1 Definition of the 1d chain, eigenmodes . . . 19
- 9.2 General framework for locally orthogonal and degenerated eigenmodes . . . 19
- 9.3 Application to the chain . . . 22

10 Dynamics of the experimental structures **24**
- 10.1 Normal modes . . . 24
- 10.2 Bifurcation scenarii . . . 24

References **27**

1 List of supplementary movies

The reader will find here a number of movies illustrating the frozen and collective actuation dynamics experimentally observed in the case of the single particle, the triangular lattice and the kagome lattice. We have also included one movie obtained from numerical simulations of the annealing dynamics from large values of π to low values of π in the case of the triangular lattice ($N = 19$), and movie from numerical simulation of large triangular and kagome lattices which demonstrate that our observations are not limited to small systems. The first video illustrates the self-alignment of an active unit toward its direction of motion.

- SI Movie 1: Alignment experiment. We impose a square motion to an active building block, and look at the response of the polarity. At each side of the square, the polarity aligns toward the new velocity vector. Acquired at 40 fps, displayed in real time.
- SI Movie 2: Experiment: translation in a triangular lattice ($N = 37$) with free boundary condition. Acquired at 30 fps, displayed in real time.
- SI Movie 3: Experiment: rotation dynamics in a triangular lattice ($N = 37$) with free boundary condition. Acquired at 30 fps, displayed in real time.
- SI Movie 4: Experiment: Frozen-Disordered dynamics in the triangular lattice ($N = 19$ active units). Acquired at 40 fps, displayed in real time.
- SI Movie 5: Experiment: Collective Actuation regime in the triangular lattice ($N = 19$ active units). Acquired at 40 fps, displayed in real time.
- SI Movie 6: Experiment: Heterogeneous regime in the triangular lattice ($N = 19$ active units). Acquired at 40 fps, displayed in real time.
- SI Movie 7: Experiment: Frozen-Disordered dynamics in the kagome lattice ($N = 12$ active units). Acquired at 40 fps, displayed in real time.
- SI Movie 8: Experiment: Collective Actuation dynamics in the kagome lattice ($N = 12$ active units). Acquired at 40 fps, displayed in real time.
- SI Movie 9: Experiment: Frozen dynamics in the single particle system. Acquired at 40 fps, displayed in real time.
- SI Movie 10: Experiment: Spontaneous oscillations in the single particle system. Acquired at 40 fps, displayed in real time.
- SI Movie 11: Numerical simulation : Annealing in π in the triangular lattice ($N = 19$ active units), with the same tension as in the experiment of SI Video 6. The elasto-active coupling π is decreased from the CA regime until the system finds a fixed point. Individual polarities are represented by a black arrow, springs are color-coded by stress state; an elongated spring turns red, while a compressed one turns blue.
- SI Movie 12: Numerical simulation of a large triangular lattice ($N = 1141$ active units), sized such that its lower energy modes have squared eigenfrequencies equal to unity. The system is initialized with zero displacement in every nodes and random initial condition for the polarities orientations, and $\pi = 2.0$. Polarities are shown as arrows colored by their orientations. Springs are represented in gray. The system quickly finds a collective actuation regime.
- SI Movie 13: Numerical simulation of a large kagome lattice ($N = 930$ active units), sized such that its lower energy modes have squared eigenfrequencies equal to unity. The system is initialized with zero displacement in every nodes and random initial condition for the polarities orientations, and $\pi = 10.0$. Polarities are shown as arrows colored by their orientations. Springs are represented in gray. The system quickly finds a collective actuation regime.

2 Model

2.1 General equations

We consider N active *self-aligning* polar particles such as those described in [1–3], connected by linear springs of stiffness k and unstressed length l_0. For each active component, the activity takes the form of a force $\boldsymbol{F}_a = F_0\hat{\boldsymbol{n}}_i$

along the polarity $\hat{\boldsymbol{n}}_i$ of the particle. The equations describing the dynamics of such a system are

$$m\frac{d\boldsymbol{v}_i}{dt} = F_0\hat{\boldsymbol{n}}_i - \gamma\boldsymbol{v}_i + \sum_{j\in\partial i} k\left(|\boldsymbol{r}_i - \boldsymbol{r}_j| - l_0\right)\hat{\boldsymbol{e}}_{ij} \tag{S1.1}$$

$$\tau\frac{d\hat{\boldsymbol{n}}_i}{dt} = \zeta(\hat{\boldsymbol{n}}_i \times \boldsymbol{v}_i) \times \hat{\boldsymbol{n}}_i + \sqrt{2\alpha}\xi\hat{\boldsymbol{n}}_i^{\perp} \tag{S1.2}$$

where m is the mass of the active particles, γ the friction coefficient, k the stiffness of the spring, and $\hat{\boldsymbol{e}}_{ij}$ the unit vector from i to j. In the absence of confinement, the particles thus move with a cruise velocity $v_0 = F_0/\gamma$. The orientation dynamics Eq. (S1.2) contains the key ingredient, specific to the model, namely the presence of a self-aligning torque of the orientation $\hat{\boldsymbol{n}}_i$ towards the velocity $\boldsymbol{v}_i$. This torque originates from the fact that the dissipative force is not symmetric with respect to the propulsion direction $\hat{\boldsymbol{n}}_i$ when $\boldsymbol{v}_i$ is not aligned with $\hat{\boldsymbol{n}}_i$. This ingredient was shown to be at the root of frozen to orbiting dynamics for a single hexbug in a harmonic trap [1], as well as of the emergence of collective motion in a system of vibrated polar discs [2,3]. Finally, the orientation dynamics contains a delta-correlated gaussian noise $\xi(t)$ with zero mean and variance $\langle\xi(t)\xi(t')\rangle = \delta(t-t')$; α/τ^2 is the rotational diffusion coefficient.

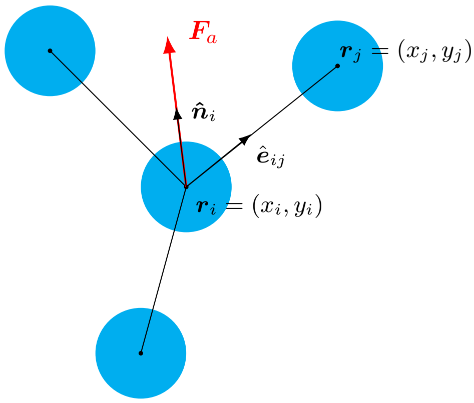

FIG. S1. Notations

Rescaling length by $r_0 = l_0$ and time by $t_0 = \gamma/k$, the characteristic time of a damped spring, the dimensionless equations of motion read

$$\tau_v\frac{d\boldsymbol{v}_i}{dt} = \tilde{F}_0\hat{\boldsymbol{n}}_i - \boldsymbol{v}_i + \sum_{j\in\partial i}\left(|\boldsymbol{r}_i - \boldsymbol{r}_j| - 1\right)\hat{\boldsymbol{e}}_{ij} \tag{S2.1}$$

$$\tau_n\frac{d\hat{\boldsymbol{n}}_i}{dt} = (\hat{\boldsymbol{n}}_i \times \boldsymbol{v}_i) \times \hat{\boldsymbol{n}}_i + \sqrt{2D}\xi\hat{\boldsymbol{n}}_i^{\perp} \tag{S2.2}$$

with four parameters, $\tau_v = mk/\gamma^2$, $\tau_n = \tau/(\zeta l_0)$, $\tilde{F}_0 = F_0/kl_0$ and $D = \alpha\gamma/k(\zeta l_0)^2$. Note that $\tau_n = l_a/l_0$ and $\tilde{F}_0 = l_e/l_0$, where $l_a = \tau/\zeta$ is the alignment length, that is the length over which the particle must move to align its orientation onto its displacement, and $l_e = F_0/k$ is the elasto-active length, which is the distance that the active force can drive away the particle from its equilibrium position, given the elastic restoring force.

In the following, as well as in the main text, we consider the set of Eqs. (S2.1) and (S2.2) while taking the over-damped limit ($\tau_v \to 0$) in the position dynamics Eq. (S2.1) and the noiseless limit of the polarity dynamics Eq. (S2.2). This leads us to the equations:

$$\frac{d\boldsymbol{r}_i}{dt} = \tilde{F}_0\hat{\boldsymbol{n}}_i + \boldsymbol{F}_i^{\mathrm{el}} \tag{S3.1}$$

$$\tau_n\frac{d\hat{\boldsymbol{n}}_i}{dt} = (\hat{\boldsymbol{n}}_i \times \boldsymbol{F}_i^{\mathrm{el}}) \times \hat{\boldsymbol{n}}_i \tag{S3.2}$$

with $\boldsymbol{F}_i^{\mathrm{el}} = \sum_{j\in\partial i}\delta l_{ij}\hat{\boldsymbol{e}}_{ij}$ the dimensionless elastic force acting on particle i, and $\delta l_{ij} = |\boldsymbol{r}_i - \boldsymbol{r}_j| - 1$, τ_n, D and $\tilde{F}_0$ being the same quantities as before. In this limit, the torque in the equation for the orientation dynamics is aligning the orientation towards the elastic force acting on the active particle.

2.2 Experimental measure of the microscopic parameters

In this section, we describe three experiments, which we conducted to measure the parameters of the hexbugs dynamics. First, we evaluate the influence of inertia and the relevance of the overdamped limit. Then we measure the alignment length l_a of one bug, our model's key parameter, as well as the angular noise D_θ. Finally we measure the active force F_0 the hexbugs are able to exert.

2.2.1 Inertia

We consider a single active particle, initially at rest, whose self-propulsion is switched on at $t = 0$ and whose orientation is fixed. This process is realized by connecting the hexbugs power supply to a DC generator with thin iron wires through a hole pierced in the middle the the PP plastic film (Fig. S2-a). The DC generator delivers a Heaviside signal of amplitude 1.5 V at $t = 0$. We use two cardboard blocker on the sides of the hexbug to prevent its polarity to rotate with respect to the annulus orientation, setting the orientation $\hat{\boldsymbol{n}}$ essentially constant. The experiments were runt 20 times, acquired at 75 fps frame rate. When the DC generator is switched on, the active unit accelerates, with its speed being given by

$$V(t) = v_0(1 - e^{-t/\tau_d}), \tag{S4}$$

where $v_0 = F_0/\gamma$ is the cruise velocity, and $\tau_d = m/\gamma = \tau_v t_0$ is the acceleration time. The values $v_0 = 20.1 \pm 0.2$ cm/s and $\tau_d = 0.12 \pm 0.01$ s are obtained from a fit of the velocity averaged over the 20 realizations. For timescales larger than τ_d, such as those considered at the level of the collective dynamics, inertia can be safely neglected.

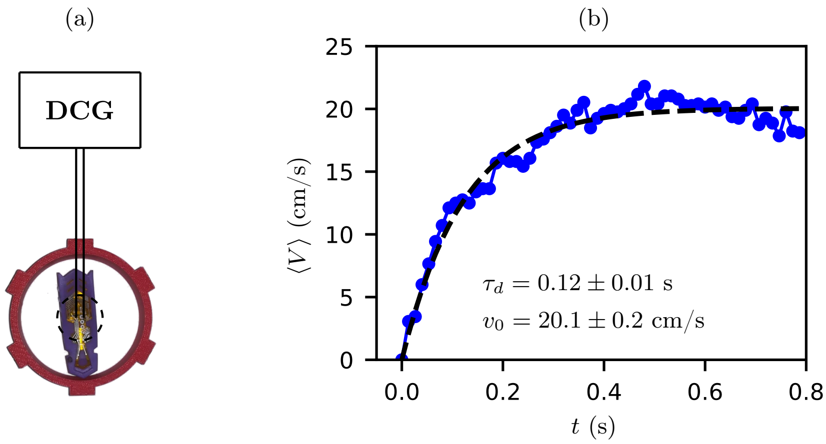

FIG. S2. **Inertia measurement.** (a) Experimental active elastic unit powered by a DC generator that delivers a Heaviside signal of amplitude 1.5 V at $t = 0$. The hexbug's polarity is fixed during the whole experiment. (b) Average speed over 20 realizations (•), fitted by Eq. (S4) (black dashed line) with a least square method.

2.2.2 Self-alignment

In order to quantify the self-alignment strength, we analyze the response of the polarity $\hat{\boldsymbol{n}}_i$ when imposing a square motion to the active unit using a XY-table. At each corner of the square, the orientation of the velocity $\boldsymbol{v}_i$ changes abruptly and the polarity aligns with the new imposed velocity. Snapshots of this process are shown in Fig. 1 of the main text for one corner of the square (Movie 1). Denoting $\phi(t)$ the angle between the polarity and the velocity vector at any time, Eq. (S1.2) reads:

$$\tau \frac{d\phi}{dt} = -V\zeta \sin(\phi) + \sqrt{2\alpha}\xi \tag{S5}$$

Where V is the imposed speed, and where we consider a fixed velocity vector. In the absence of noise, the solution to the initial condition problem with $\phi(t=0) = \phi_0 = 90°$, is

$$\tan\left(\frac{\phi(t)}{2}\right) = \tan\left(\frac{\phi_0}{2}\right) \exp\left(-\frac{t}{\tau_a}\right), \tag{S6}$$

where the alignement time is $\tau_a = l_a/V$. In the presence of noise, the Fokker-Planck equation associated to Eq. (S5) is

$$\frac{\partial P}{\partial t}(\phi, t) = \frac{\partial}{\partial \phi}\left(\frac{V\zeta}{\tau} \sin(\phi) P(\phi, t)\right) + \frac{\partial^2}{\partial \phi^2}\left(\frac{\alpha}{\tau^2} P(\phi, t)\right), \tag{S7}$$

where $P(\phi, t)$ is the probability distribution of the angle ϕ at time t. The stationary probability density $P_{ss}(\phi)$ satisfies:

$$\frac{d^2 P_{ss}}{d\phi^2}(\phi) + \sin(\phi)\frac{V\zeta\tau}{\alpha}\frac{dP_{ss}}{d\phi}(\phi) + \cos(\phi)\frac{V\zeta\tau}{\alpha}P_{ss}(\phi) = 0, \tag{S8}$$

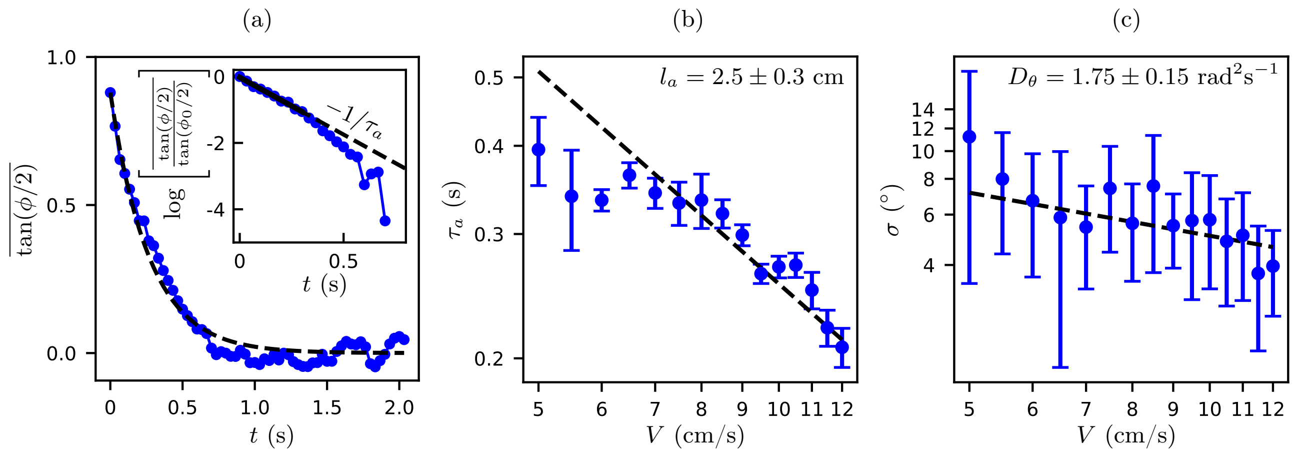

FIG. S3. **Self-alignment experiments.** (a) Average misalignment $\overline{\tan(\phi/2)}(t) = \sum_i \tan(\phi_i/2)(t)/N$ of 10 independent realizations with $V = 10$ cm/s (•), superposed with Eq. (S6) (black dashed line). Inset: τ_a is measured by fitting the short times of $\tan(\phi(t)/2) / \tan(\phi_0/2)$ with an exponential decay. (b) Alignment time τ_a as a function of the imposed speed V (•). Vertical errorbars are given by the 1-σ confidence intervals. We show an inverse function (black dotted line) which prefactor gives an estimate of the alignment length l_a (c) Averaged standard deviation σ of missalignment as a function of the imposed speed V (•). It is measured by averaging the standard deviations of missalignments for 10 realizations at a given speed. Data are analysed after two associated τ_a to considered only the stationnary distributions. Vertical errorbars are given by the standard deviation of the standard deviations for each speed. We fit the data with Eq. (S10) (black dashed line).

which has the following solution:

$$P_{ss}(\phi) = \mathcal{N} \exp\left(\frac{V\zeta\tau}{\alpha}\cos(\phi)\right). \tag{S9}$$

where $\mathcal{N}$ is a normalization factor. In the vicinity of $\phi = 0$, this distribution is a Gaussian with a standard deviation

$$\sigma = \sqrt{\frac{\alpha}{\tau\zeta V}} = \sqrt{\frac{D_\theta l_a}{V}}, \tag{S10}$$

where $D_\theta = \alpha/\tau^2$ is the angular diffusion coefficient.

Experimentally, we set the motion speed from 5 cm/s to 12 cm/s (upper limit of the XY table), by steps of 0.5 cm/s and perform 10 independent realizations for each speed value, that we acquire at 40 fps. The average response for a speed $V = 10$ cm/s is shown in Fig. S3(a), and illustrate the transitory regime.

The alignment time, τ_a, is obtained by fitting the initial decay of $\tan\left(\frac{\phi(t)}{2}\right) / \tan\left(\frac{\phi_0}{2}\right)$, averaged over the realizations, and plotted as a function of the imposed speed V on Fig. S3(b). For large enough speed, where the relative importance of the noise is weaker, τ_a decreases as $1/V$, in agreement with Eq. (S6), and we extract an alignment length $l_a = 2.5 \pm 0.3$ cm.

As seen from Fig. S3(c), the standard deviation of the misalignment fluctuations, measured in the steady regime, is observed to decay is a way that is consistent with the prediction of Eq. (S10). This allows us to extract an angular diffusion constant $D_\theta = 1.75 \pm 0.15$ rad$^2 s^{-1}$.

2.2.3 Active force

To evaluate the active force we restrict the motion of an elementary active elastic unit by putting it in a sufficiently thin rectangular channel, and we fix the hexbug polarity so that it always points in the long direction of the arena, as shown in Fig. 1 of the main text. The active unit is attached to one end of the channel by a spring. As activity is switched on, the hexbug moves in the forward direction up to the point where the elastic force balances the active one. As we know the spring's stiffness, the extension of the spring in the steady state gives a measure of the active force $F_0 = 43 \pm 3$ mN. The uncertainty is given by the standard deviation of the measure on 5 different hexbugs. Having extracted F_0, we can obtain the elastic length $l_e = F_0/k$ for the springs of different stiffness that we use. Together with l_a, we are therefore in position to have the experimental value for $\pi = l_e/l_a$, the central control parameter of the experiment.

3 The harmonic approximation

3.1 Formulation of the harmonic approximation using Bra-ket notations

As we shall see below, it will be useful to recast Eqs. (S3) using bra-ket notations:

$$|\dot{\boldsymbol{r}}\rangle = \tilde{F}_0|\hat{\boldsymbol{n}}\rangle + |\boldsymbol{F}^{\mathrm{el}}\rangle \tag{S11.1}$$

$$\tau_n|\dot{\theta}\rangle = \mathbb{K}|\boldsymbol{F}^{\mathrm{el}}\rangle \tag{S11.2}$$

where $\langle i|\boldsymbol{a}\rangle = \boldsymbol{a}_i$, and where the matrix $\mathbb{K}$ has dimension $N \times 2N$, with elements $\langle i|\mathbb{K}|j\rangle = \hat{\boldsymbol{n}}_i^{\perp}\delta_{ij}$, which explicitly depends on the polarity field configuration $|\hat{\boldsymbol{n}}\rangle$. We also introduce the displacement field $|\boldsymbol{u}\rangle$, defined as the displacement with respect to the reference configuration $|\boldsymbol{R}\rangle$, $|\boldsymbol{r}\rangle = |\boldsymbol{R}\rangle + |\boldsymbol{u}\rangle$, as done in the Cauchy-Born theory of elastic solids [6].

The harmonic approximation consists in linearizing the elastic force for small gradients of displacement [6]:

$$|\boldsymbol{F}^{\mathrm{el}}\rangle = -\mathbb{M}|\boldsymbol{u}\rangle \tag{S12}$$

where $\mathbb{M}$ is called the dynamical matrix, which is square, real and symmetric. Thus one can find a complete orthonormal basis in which it is diagonal, namely the normal modes $|\boldsymbol{\varphi}_k\rangle$, with corresponding eigenvalues ω_k^2, the squared frequencies of vibrations, also called the modes' energies. By convention, we sort the eigenvalues from the smallest to the largest $\omega_1^2 \leq ... \leq \omega_i^2 \leq \cdots \leq \omega_{dN}^2$, with N the number of particles, and $d = 2$ the space dimensin. Note that in an overdamped elastic model, the denomination *squared eigenfrequencies* is misleading as the projection of the displacement field on the mode $|\boldsymbol{\varphi}_k\rangle$ does not oscillate at frequency ω_k, but relaxes to the reference configuration on a typical time $1/\omega_k^2$. The structures considered in this work are mechanically stable [5]: $\mathbb{M}$ is positive definite, and all normal modes have a finite energy $\omega_k^2 > 0$.

Combining Eqs. (S11) and (S12) and rescaling $\boldsymbol{u} \to \tau_n \boldsymbol{u}$, we end up with a system of equations :

$$|\dot{\boldsymbol{u}}\rangle = \pi|\hat{\boldsymbol{n}}\rangle - \mathbb{M}|\boldsymbol{u}\rangle, \tag{S13.1}$$

$$|\dot{\theta}\rangle = -\mathbb{K}\mathbb{M}|\boldsymbol{u}\rangle, \tag{S13.2}$$

or equivalently

$$|\dot{\boldsymbol{u}}\rangle = \pi|\hat{\boldsymbol{n}}\rangle - \mathbb{M}|\boldsymbol{u}\rangle \tag{S14.1}$$

$$|\dot{\boldsymbol{n}}\rangle = -\mathbb{K}^T\mathbb{K}\mathbb{M}|\boldsymbol{u}\rangle \tag{S14.2}$$

where $\pi = \tilde{F}_0/\tau_n = F_0/kl_a = l_e/l_a$ is the only dimensionless parameter of the problem.

3.2 Projection on the normal modes

Decomposing the displacement and polarity fields:

$$|\boldsymbol{u}\rangle = \sum_k a_k^u|\boldsymbol{\varphi}_k\rangle \tag{S15.1}$$

$$|\hat{\boldsymbol{n}}\rangle = \sum_k a_k^n|\boldsymbol{\varphi}_k\rangle, \tag{S15.2}$$

the equations of motion (S14) translate into

$$\frac{da_k^u}{dt} = \pi a_k^n - \omega_k^2 a_k^u, \tag{S16.1}$$

$$\frac{da_k^n}{dt} = -\sum_{lpq}\omega_q^2\Gamma_{pqlk}a_q^u a_l^n a_p^n, \tag{S16.2}$$

where we have introduced the coupling coefficients

$$\Gamma_{pqlk} = \sum_i \boldsymbol{\varphi}_k^i \cdot \left[(\boldsymbol{\varphi}_p^i \times \boldsymbol{\varphi}_q^i) \times \boldsymbol{\varphi}_l^i\right] = \sum_i \left[\boldsymbol{\varphi}_p^i \times \boldsymbol{\varphi}_q^i\right] \cdot \left[\boldsymbol{\varphi}_l^i \times \boldsymbol{\varphi}_k^i\right], \tag{S17}$$

with $\boldsymbol{\varphi}_k^i = \langle i|\boldsymbol{\varphi}_k\rangle$, the component of the mode $|\boldsymbol{\varphi}_k\rangle$ on the node i. One notices the strong nonlinearity of the second equation, inherited from the self-alignment dynamics of the polarity. The coupling coefficients Γ_{pqlk} are antisymmetric under the exchanges $p \leftrightarrow q$ and $l \leftrightarrow k$, and symmetric under the exchange $(p, q) \leftrightarrow (l, k)$. This implies for instance that $\sum_{pl}\Gamma_{pqlk}a_l^n a_p^n$ is symmetric under the exchange $k \leftrightarrow q$.

In addition to the dynamical equation, the normalization condition $|\hat{\boldsymbol{n}}_i| = 1$ for all i implies that the $2N$ polarity coefficients a_k^n belong to a N-dimensional manifold isomorphic to the N-torus. Since the normalization condition implies that $\sum_i \boldsymbol{n}_i^2 = \sum_k a_k^{n\,2} = N$, this manifold is included in the $(2N-1)$-sphere of radius $\sqrt{N}$.

4 Fixed points stability analysis

4.1 An infinite set of fixed points

Equilibrium configurations of Eqs. (S13) are given by:

$$\pi|\hat{\boldsymbol{n}}\rangle - \mathbb{M}|\boldsymbol{u}\rangle = 0 \tag{S18a}$$
$$\mathbb{K}\mathbb{M}|\boldsymbol{u}\rangle = 0 \tag{S18b}$$

Eq. (S18a) imposes $|\boldsymbol{u}\rangle = \pi\mathbb{M}^{-1}|\hat{\boldsymbol{n}}\rangle$; then Eq. (S18b) is always satisfied since $\mathbb{K}|\hat{\boldsymbol{n}}\rangle = 0$ by construction: to any configuration of the polarity field $|\hat{\boldsymbol{n}}\rangle$ corresponds the fixed point $\{|\boldsymbol{u}\rangle = \pi\mathbb{M}^{-1}|\hat{\boldsymbol{n}}\rangle, |\hat{\boldsymbol{n}}\rangle\}$. The set of fixed points is thus isomorphic to the N-torus.

4.2 Dynamics linearized around a given fixed point

To study the stability of a given fixed point $\{|\boldsymbol{u}^0\rangle, |\hat{\boldsymbol{n}}^0\rangle\}$ we consider small perturbations $|\hat{\boldsymbol{n}}\rangle = |\hat{\boldsymbol{n}}^0\rangle + |\boldsymbol{\delta}\hat{\boldsymbol{n}}\rangle$ and $|\boldsymbol{u}\rangle = |\boldsymbol{u}^0\rangle + |\boldsymbol{\delta u}\rangle$, where $\hat{\boldsymbol{n}}_i^0 = (\cos\theta_i^0, \sin\theta_i^0)$ and $\boldsymbol{\delta}\hat{\boldsymbol{n}}_i = (-\sin\theta_i^0, \cos\theta_i^0)\delta\theta_i = \hat{\boldsymbol{n}}_i^{0\perp}\delta\theta_i = \langle i|\mathbb{K}_0^T|\delta\theta\rangle$. Linearizing Eqs. (S13) one gets:

$$|\dot{\boldsymbol{\delta u}}\rangle = -\mathbb{M}|\boldsymbol{\delta u}\rangle + \pi\mathbb{K}_0^T|\delta\theta\rangle \tag{S19.1}$$
$$|\dot{\delta\theta}\rangle = -\mathbb{K}_0\mathbb{M}|\boldsymbol{\delta u}\rangle - \pi\delta\mathbb{K}|\hat{\boldsymbol{n}}^0\rangle \tag{S19.2}$$

Since $\boldsymbol{\delta}\hat{\boldsymbol{n}}_i^\perp = (-\cos\theta_i^0, -\sin\theta_i^0)\delta\theta_i = -\hat{\boldsymbol{n}}_i^0\delta\theta_i$, we use the contraction $\delta\mathbb{K}|\hat{\boldsymbol{n}}^0\rangle = -|\delta\theta\rangle$. Finally, rescaling $t \to \pi^{-1}t$ leads to the following system:

$$|\dot{\boldsymbol{\delta u}}\rangle = -\pi^{-1}\mathbb{M}|\boldsymbol{\delta u}\rangle + \mathbb{K}_0^T|\delta\theta\rangle \tag{S20.1}$$
$$|\dot{\delta\theta}\rangle = -\pi^{-1}\mathbb{K}_0\mathbb{M}|\boldsymbol{\delta u}\rangle + |\delta\theta\rangle \tag{S20.2}$$

Therefore the stability of the configuration $|\hat{\boldsymbol{n}}^0\rangle$ is encoded in the $3N$ eigenvalues of the matrix

$$\mathbb{D} = \begin{pmatrix} -\pi^{-1}\mathbb{M} & \mathbb{K}_0^T \\ -\pi^{-1}\mathbb{K}_0\mathbb{M} & \mathbb{I} \end{pmatrix} \tag{S21}$$

The matrix $\mathbb{D}$ depends on the parameter π, the network geometry, and the equilibrium configuration of the polarities encoded in the matrix $\mathbb{K}_0$. In the following we drop the subscript 0, but one should remember that $\mathbb{K}$ depends on the configuration of the polarities.

4.3 Properties of the spectrum valid for all fixed points

Consider the eigenvector $|\Psi\rangle = (|\boldsymbol{b}\rangle, |\boldsymbol{c}\rangle)$ of the matrix $\mathbb{D}$ with eigenvalue λ, then:

$$-\pi^{-1}\mathbb{M}|\boldsymbol{b}\rangle + \mathbb{K}^T|\boldsymbol{c}\rangle = \lambda|\boldsymbol{b}\rangle, \tag{S22a}$$
$$-\pi^{-1}\mathbb{K}\mathbb{M}|\boldsymbol{b}\rangle + |\boldsymbol{c}\rangle = \lambda|\boldsymbol{c}\rangle. \tag{S22b}$$

Multiplying Eq. (S22a) by $\mathbb{K}$ and noting that $\mathbb{K}\mathbb{K}^T = \mathbb{I}$ leads to:

$$-\pi^{-1}\mathbb{K}\mathbb{M}|\boldsymbol{b}\rangle + |\boldsymbol{c}\rangle = \lambda\mathbb{K}|\boldsymbol{b}\rangle. \tag{S23}$$

Comparing with Eq. (S22b), we obtain that either $\mathbb{K}|\boldsymbol{b}\rangle = |\boldsymbol{c}\rangle$ or $\lambda = 0$.

- First, we consider the case $\lambda = 0$. From Eq. (S23), $|\boldsymbol{c}\rangle = \pi^{-1}\mathbb{K}\mathbb{M}|\boldsymbol{b}\rangle$; using this relation in Eq. (S22a) leads to

  $$\left(\mathbb{I} - \mathbb{K}^T\mathbb{K}\right)\mathbb{M}|\boldsymbol{b}\rangle = 0. \tag{S24}$$

  This means that $\mathbb{M}|\boldsymbol{b}\rangle$ must be an eigenvector of $\mathbb{K}^T\mathbb{K}$ with eigenvalue 1. The operator $\mathbb{K}^T\mathbb{K}$ is the projector on the space spanned by $(|\hat{\boldsymbol{n}}_i^\perp\rangle)_i$: it has N eigenvectors $|\boldsymbol{\kappa}_i\rangle = |\hat{\boldsymbol{n}}_i\rangle = \hat{\boldsymbol{n}}_i|i\rangle$ with eigenvalue 0 and N eigenvectors $|\boldsymbol{\kappa}_i\rangle = |\hat{\boldsymbol{n}}_i^\perp\rangle = \hat{\boldsymbol{n}}_i^\perp|i\rangle$ with eigenvalue 1.

  Hence, for any equilibrium configuration, there are N eigenvectors with eigenvalue 0, given by

  $$|\boldsymbol{b}\rangle = \mathbb{M}^{-1}\hat{\boldsymbol{n}}_i^\perp|i\rangle \tag{S25a}$$
  $$|\boldsymbol{c}\rangle = \pi^{-1}|i\rangle. \tag{S25b}$$

  These eigenvectors span the tangent space of the N dimensional fixed points manifold. We also note that as a consequence the equilibrium configurations are all marginally stable.

- Second, we consider the case $\mathbb{K}|\boldsymbol{b}\rangle = |\boldsymbol{c}\rangle$. Inserting this relation in Eq. (S22a), we obtain

$$\left(-\pi^{-1}\mathbb{M} + \mathbb{K}^T\mathbb{K}\right)|\boldsymbol{b}\rangle = \lambda|\boldsymbol{b}\rangle. \tag{S26}$$

  λ should thus be an eigenvalue of the symmetric matrix

$$\tilde{\mathbb{D}} = -\pi^{-1}\mathbb{M} + \mathbb{K}^T\mathbb{K}. \tag{S27}$$

Since $\tilde{\mathbb{D}}$ is symmetric, λ is real; hence, the spectrum of $\mathbb{D}$, Spec($\mathbb{D}$), is real and is given by

$$\mathrm{Spec}(\mathbb{D}) = \{0\} \cup \mathrm{Spec}\left(\tilde{\mathbb{D}}\right). \tag{S28}$$

Since the eigenvalues of $\mathbb{M}$ are bounded between ω_{min}^2 and ω_{max}^2, and the eigenvalues of $\mathbb{K}^T\mathbb{K}$ are 0 and 1, the eigenvalues of $\tilde{\mathbb{D}}$ are bounded by

$$-\frac{\omega_{\mathrm{max}}^2}{\pi} \le \mathrm{Spec}\left(\tilde{\mathbb{D}}\right) \le 1 - \frac{\omega_{\mathrm{min}}^2}{\pi}. \tag{S29}$$

When $\pi \to 0$, we see from Eq. (S29) that Spec($\tilde{\mathbb{D}}$) $\to -\infty$. When $\pi \to \infty$, $\tilde{\mathbb{D}} \to \mathbb{K}^T\mathbb{K}$, which has eigenvalues 0 and 1 with N associated eigenvectors each.

4.4 Stability threshold of a given fixed point

A given fixed point is stable if Spec($\tilde{\mathbb{D}}$) ≤ 0, which is equivalent to the fact that for any vector $|\boldsymbol{b}\rangle$,

$$\langle\boldsymbol{b}|\tilde{\mathbb{D}}|\boldsymbol{b}\rangle \le 0. \tag{S30}$$

With the explicit expression of $\tilde{\mathbb{D}}$, this reads

$$\langle\boldsymbol{b}| - \pi^{-1}\mathbb{M} + \mathbb{K}^T\mathbb{K}|\boldsymbol{b}\rangle \le 0. \tag{S31}$$

We now project $|\boldsymbol{b}\rangle$ on the eigenvectors of $\mathbb{M}$; denoting $b_k = \langle\boldsymbol{\varphi}_k|\boldsymbol{b}\rangle$, this reads

$$\sum_{jk} b_j b_k \left(-\pi^{-1}\omega_j\omega_k + \langle\boldsymbol{\varphi}_j|\mathbb{K}^T\mathbb{K}|\boldsymbol{\varphi}_k\rangle\right) \le 0. \tag{S32}$$

Now defining $\tilde{b}_k = \omega_k b_k$, this becomes

$$\sum_{jk} \tilde{b}_j\tilde{b}_k \left(-\pi^{-1} + \frac{\langle\boldsymbol{\varphi}_j|\mathbb{K}^T\mathbb{K}|\boldsymbol{\varphi}_k\rangle}{\omega_j\omega_k}\right) \le 0. \tag{S33}$$

Introducing the matrix

$$\mathbb{L}_{jk} = \frac{\langle\boldsymbol{\varphi}_j|\mathbb{K}^T\mathbb{K}|\boldsymbol{\varphi}_k\rangle}{\omega_j\omega_k}, \tag{S34}$$

the stability condition reads

$$\mathrm{Spec}\left(-\pi^{-1}\mathbb{I} + \mathbb{L}\right) \le 0. \tag{S35}$$

But $\mathrm{Spec}\left(-\pi^{-1}\mathbb{I} + \mathbb{L}\right) = -\pi^{-1} + \mathrm{Spec}(\mathbb{L})$. Finally, the fixed point $|\hat{\boldsymbol{n}}\rangle$ is stable if

$$\pi \le \pi_c\left(|\hat{\boldsymbol{n}}\rangle\right) = \frac{1}{\max\mathrm{Spec}\left(\mathbb{L}\left(|\hat{\boldsymbol{n}}\rangle\right)\right)}. \tag{S36}$$

4.5 First linear destabilization

We first determine a lower bound of the stability thresholds and then show that this bound is sharp.

Let π_c^{min} be the smallest value of π for which there exists an unstable configuration. We thus have $\pi_c\left(|\hat{\boldsymbol{n}}\rangle\right) \ge \pi_c^{\mathrm{min}}$ for all $|\hat{\boldsymbol{n}}\rangle$. From Eq. (S29) there can be a positive eigenvalue only if $\pi > \omega_{\mathrm{min}}^2$, hence we have

$$\pi_c\left(|\hat{\boldsymbol{n}}\rangle\right) \ge \pi_c^{\mathrm{min}} = \omega_{\mathrm{min}}^2. \tag{S37}$$

We now exhibit a configuration $|\hat{\boldsymbol{n}}_{\mathrm{min}}\rangle$ that does destabilize at ω_{min}^2. Consider the eigenmode of $\mathbb{M}$ associated to the eigenvalue $\omega_1^2 = \omega_{\mathrm{min}}^2$, $|\boldsymbol{\varphi}_1\rangle$; and a configuration $|\hat{\boldsymbol{n}}_{\mathrm{min}}\rangle$ where the orientation $\hat{\boldsymbol{n}}_i$ is orthogonal to $\boldsymbol{\varphi}_1^i$ for every particle i. For this configuration, $\mathbb{L}_{11} = \omega_{\mathrm{min}}^{-2}$, hence $\max\mathrm{Spec}(\mathbb{L}) \ge \omega_{\mathrm{min}}^{-2}$ and $\pi_c(|\hat{\boldsymbol{n}}\rangle) \le \omega_{\mathrm{min}}^2$. With the lower bound (S37), we conclude that $\pi_c^{\mathrm{min}} = \pi_c(|\hat{\boldsymbol{n}}_{\mathrm{min}}\rangle) = \omega_{\mathrm{min}}^2$: the lower bound (S37) is sharp and the first configuration to destabilize is related to the lowest energy mode in a simple way.

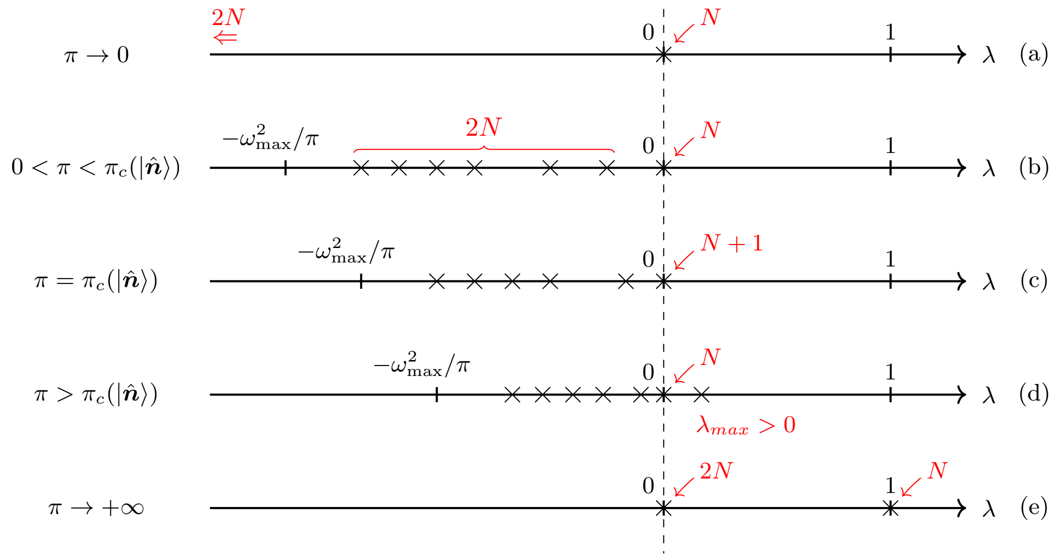

FIG. S4. **Eigenvalue spectrum for an arbitrary fixed point $\{|\boldsymbol{u}\rangle = \pi\mathbb{M}^{-1}|\hat{\boldsymbol{n}}\rangle, |\hat{\boldsymbol{n}}\rangle\}$.** The fixed point is stable for $\pi < \pi_c(|\hat{\boldsymbol{n}}\rangle)$, where $\pi_c(|\hat{\boldsymbol{n}}\rangle)$ is given by Eqs. (S36). (a) $\pi \to 0$, N zero eigenvalues and the $2N$ which are left are strictly negative, given by $-\omega_k^2/\pi$. (b) $0 < \pi < \pi_c(|\hat{\boldsymbol{n}}\rangle)$, N zero eigenvalues, and the $2N$ which are left are strictly negative. (c) $\pi = \pi_c(|\hat{\boldsymbol{n}}\rangle)$, $N+1$ zero eigenvalues, and the $2N-1$ which are left are strictly negative. (d) $\pi > \pi_c(|\hat{\boldsymbol{n}}\rangle)$, the greatest eigenvalue is strictly positive. (e) $\pi \to +\infty$, $2N$ zero eigenvalues, N one eigenvalues.

4.6 Upper bound of the stability thresholds

We don't have an explicit analytical expression for the largest destabilization threshold, $\pi_c^{\max}$, but we can determine an upper bound π_c^{upp} of it above which there exists no stable fixed point.

To do so, we look for a $|\hat{\boldsymbol{n}}\rangle$-independent lower bound of the maximal eigenvalue of $\tilde{\mathbb{D}}$. We use the restriction of the matrix $\tilde{\mathbb{D}}$ to the two modes j and k, which is a 2×2 matrix that we denote $\tilde{\mathbb{D}}_{\{j,k\}}$. We have

$$\max\operatorname{Spec}\left(\tilde{\mathbb{D}}\left(|\hat{\boldsymbol{n}}\rangle\right)\right) \geq \max\operatorname{Spec}\left(\tilde{\mathbb{D}}_{\{j,k\}}\left(|\hat{\boldsymbol{n}}\rangle\right)\right) = \frac{\tilde{\mathbb{D}}_{jj}+\tilde{\mathbb{D}}_{kk}}{2} + \sqrt{\frac{(\tilde{\mathbb{D}}_{jj}-\tilde{\mathbb{D}}_{kk})^2}{4}+\tilde{\mathbb{D}}_{jk}^2} \geq \frac{\tilde{\mathbb{D}}_{jj}+\tilde{\mathbb{D}}_{kk}}{2}. \tag{S38}$$

Explicitly,

$$\frac{\tilde{\mathbb{D}}_{jj}+\tilde{\mathbb{D}}_{kk}}{2} = -\frac{\omega_j^2+\omega_k^2}{2\pi} + \frac{1}{2}\left(\langle\boldsymbol{\varphi}_j|\mathbb{K}^T\mathbb{K}|\boldsymbol{\varphi}_j\rangle + \langle\boldsymbol{\varphi}_k|\mathbb{K}^T\mathbb{K}|\boldsymbol{\varphi}_k\rangle\right) \tag{S39}$$

$$= -\frac{\omega_j^2+\omega_k^2}{2\pi} + \frac{1}{2}\sum_i\left[(\boldsymbol{\varphi}_j^i\times\hat{\boldsymbol{n}}_i)^2 + (\boldsymbol{\varphi}_k^i\times\hat{\boldsymbol{n}}_i)^2\right] \tag{S40}$$

Now we have to minimize the term in the sum over the orientations $\hat{\boldsymbol{n}}_i$. This amounts to find the minimal eigenvalue of the matrix

$$\boldsymbol{\varphi}_j^i\left(\boldsymbol{\varphi}_j^i\right)^T + \boldsymbol{\varphi}_k^i\left(\boldsymbol{\varphi}_k^i\right)^T = \begin{pmatrix} \left(\varphi_{j,x}^i\right)^2 + \left(\varphi_{k,x}^i\right)^2 & \left(\varphi_{j,x}^i\right)\left(\varphi_{j,y}^i\right) + \left(\varphi_{k,x}^i\right)\left(\varphi_{k,y}^i\right) \\ \left(\varphi_{j,x}^i\right)\left(\varphi_{j,y}^i\right) + \left(\varphi_{k,x}^i\right)\left(\varphi_{k,y}^i\right) & \left(\varphi_{j,y}^i\right)^2 + \left(\varphi_{k,y}^i\right)^2 \end{pmatrix} = \begin{pmatrix} c_{11} & c_{12} \\ c_{12} & c_{22} \end{pmatrix}, \tag{S41}$$

which is

$$\lambda_{\min} = \frac{1}{2}\left[c_{11}+c_{22}-\sqrt{\left(c_{11}-c_{22}\right)^2+4c_{12}^2}\right] \tag{S42}$$

$$= \frac{1}{2}\left[\left(\boldsymbol{\varphi}_j^i\right)^2 + \left(\boldsymbol{\varphi}_k^i\right)^2 - \left(\left[\left(\boldsymbol{\varphi}_j^i\right)^2 + \left(\boldsymbol{\varphi}_k^i\right)^2\right]^2 - 4\left[\boldsymbol{\varphi}_j^i\times\boldsymbol{\varphi}_k^i\right]^2\right)^{1/2}\right]. \tag{S43}$$

Using the fact that the modes are normalized, we finally get the bound

$$\max\operatorname{Spec}\left(\tilde{\mathbb{D}}\left(|\hat{\boldsymbol{n}}\rangle\right)\right) \geq -\frac{\omega_j^2+\omega_k^2}{2\pi} + \frac{1}{2}\left[1-\frac{1}{2}\sum_i\left(\left[\left(\boldsymbol{\varphi}_j^i\right)^2 + \left(\boldsymbol{\varphi}_k^i\right)^2\right]^2 - 4\left[\boldsymbol{\varphi}_j^i\times\boldsymbol{\varphi}_k^i\right]^2\right)^{1/2}\right], \tag{S44}$$

All the fixed points are unstable when this bound is positive, which happens for

$$\pi \geq \pi_{c,u}^{\{j,k\}} = \frac{\omega_j^2+\omega_k^2}{c(|\boldsymbol{\varphi}_j\rangle, |\boldsymbol{\varphi}_k\rangle)}, \tag{S45}$$

with

$$c(|\boldsymbol{\varphi}_j\rangle, |\boldsymbol{\varphi}_k\rangle) = 1 - \frac{1}{2}\sum_i \left(\left[\left(\boldsymbol{\varphi}_j^i\right)^2 + \left(\boldsymbol{\varphi}_k^i\right)^2 \right]^2 - 4\left[\boldsymbol{\varphi}_j^i \times \boldsymbol{\varphi}_k^i\right]^2 \right)^{1/2} \tag{S46}$$

Finally the bound for π, above which there exists no stable fixed point is

$$\pi_c^{\mathrm{upp}} = \min_{\{j,k\}} \left(\frac{\omega_j^2 + \omega_k^2}{c(|\boldsymbol{\varphi}_j\rangle, |\boldsymbol{\varphi}_k\rangle)} \right), \tag{S47}$$

Note that the function $c(\bullet, \bullet)$ is bounded between 0, when $j = k$ and 1, when the pair of modes $(|\boldsymbol{\varphi}_j\rangle, |\boldsymbol{\varphi}_k\rangle)$ are locally orthogonal and of the same norm.

5 One particle dynamics

The aim of this section is to study the different dynamical regimes and fixed points of Eqs. (S16) in the case of a system of one particle in dimension $d = 2$, which consequently has two eigenmodes. We note these eigenmodes $|\boldsymbol{\varphi}_1\rangle$ and $|\boldsymbol{\varphi}_2\rangle$ (respectively along $\hat{\boldsymbol{x}}$ and $\hat{\boldsymbol{y}}$), with corresponding eigenvalues ω_1^2 and ω_2^2. We decompose $|\boldsymbol{u}\rangle = a_1^u(t)|\boldsymbol{\varphi}_1\rangle + a_2^u(t)|\boldsymbol{\varphi}_2\rangle$ and $|\hat{\boldsymbol{n}}\rangle = a_1^n(t)|\boldsymbol{\varphi}_1\rangle + a_2^n(t)|\boldsymbol{\varphi}_2\rangle$. The fact that there is only one particle simplifies the problem:

- There is only one normalization condition ${a_1^n}^2 + {a_2^n}^2 = 1$.
- The only non-zero coupling coefficients are

$$\Gamma_{1212} = -\Gamma_{2112} = -\Gamma_{1221} = \Gamma_{2121} = \Gamma = \sum_i \left(\boldsymbol{\varphi}_1^i \times \boldsymbol{\varphi}_2^i\right)^2 = 1.$$

5.1 Governing ODEs

5.1.1 General case

Using the above simplification in Eqs. (S16), we find the ODEs governing the amplitude of the displacement and polarities on each mode:

$$\dot{a}_1^u = \pi a_1^n - \omega_1^2 a_1^u, \tag{S48.1}$$
$$\dot{a}_2^u = \pi a_2^n - \omega_2^2 a_2^u, \tag{S48.2}$$
$$\dot{a}_1^n = -\left(\omega_1^2 a_1^u a_2^n - \omega_2^2 a_2^u a_1^n\right) a_2^n, \tag{S48.3}$$
$$\dot{a}_2^n = \left(\omega_1^2 a_1^u a_2^n - \omega_2^2 a_2^u a_1^n\right) a_1^n. \tag{S48.4}$$

5.1.2 Degenerate case

In the degenerate case, $\omega_1^2 = \omega_2^2 = \omega_0^2$, it is more convenient to use polar coordinates. We introduce R, φ and θ such that $a_1^u = R\cos(\varphi)$, $a_2^u = R\sin(\varphi)$, $a_1^n = \cos(\theta)$ and $a_2^n = \sin(\theta)$. Using $\gamma = \theta - \varphi$, Eqs. (S48) become:

$$\dot{R} = \pi\cos(\gamma) - \omega_0^2 R, \tag{S49.1}$$
$$\dot{\varphi} = \frac{\pi}{R}\sin(\gamma), \tag{S49.2}$$
$$\dot{\gamma} = \left(\omega_0^2 R - \frac{\pi}{R}\right)\sin(\gamma). \tag{S49.3}$$

5.2 Fixed Points

5.2.1 General case

We use the polar angle of the polarity θ, such that $a_1^n = \cos(\theta)$ and $a_2^n = \sin(\theta)$. The fixed points are given by

$$\omega_1^2 a_1^u = \pi\cos(\theta_0), \tag{S50a}$$
$$\omega_2^2 a_2^u = \pi\sin(\theta_0), \tag{S50b}$$

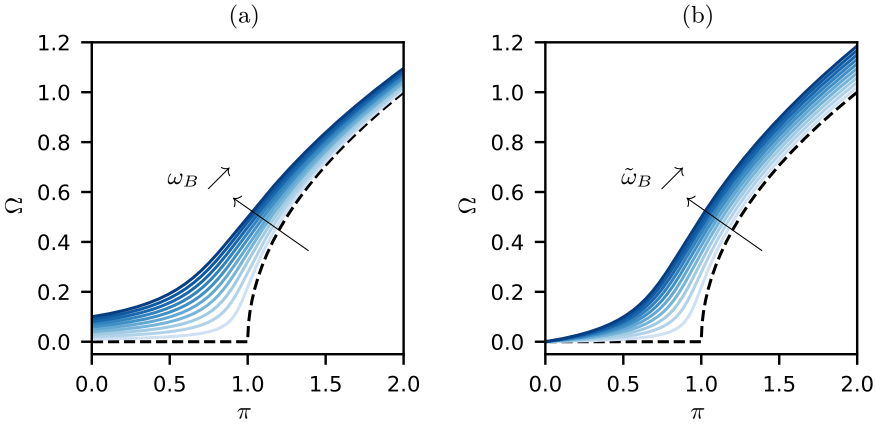

FIG. S5. **Biased single parabola.** (a) Ω as a function of π for increasing dimensionless biases $\omega_B \in [0.01, 0.02, 0.03, 0.04, 0.05, 0.06, 0.07, 0.08, 0.09, 0.1]$ (blue solid lines) compared to the unbiased case of Eq. (S54) (black dashed line). (b) Ω as a function of π for increasing dimensional bias $\tilde{\omega}_B \in [0.01, 0.02, 0.03, 0.04, 0.05, 0.06, 0.07, 0.08, 0.09, 0.1]$ (blue solid lines) compared to the unbiased case of Eq. (S54) (black dashed line). Here we use $l_a/v_0 = 1$.

for any orientation θ_0. The stability of the fixed points can be determined with Eq. (S36). The matrix $\mathbb{L}$ (Eq. (S34)) reads

$$\mathbb{L} = \begin{pmatrix} \frac{\sin(\theta_0)^2}{\omega_1^2} & -\frac{\cos(\theta_0)\sin(\theta_0)}{\omega_1\omega_2} \\ -\frac{\cos(\theta_0)\sin(\theta_0)}{\omega_1\omega_2} & \frac{\cos(\theta_0)^2}{\omega_2^2} \end{pmatrix}; \tag{S51}$$

its eigenvalues are 0 and $\frac{\sin(\theta_0)^2}{\omega_1^2} + \frac{\cos(\theta_0)^2}{\omega_2^2}$, so that this state is stable for

$$\pi \leq \pi_c(\theta_0) = \frac{\omega_1^2\omega_2^2}{\omega_2^2\sin(\theta_0)^2 + \omega_1^2\cos(\theta_0)^2}. \tag{S52}$$

5.2.2 Degenerate case

In the degenerate case, the fixed points are given by $R = \pi/\omega_0^2$, $\phi = \theta = \theta_0$. The rotational symmetry ensures that they are all equivalent and stable for

$$\pi \leq \pi_c = \omega_0^2. \tag{S53}$$

5.3 Orbiting solutions in the degenerate case

Orbiting solutions are defined by $\dot{R} = 0$, $\dot{\gamma} = 0$ and $\dot{\varphi} = \Omega \neq 0$. From Eqs. (S49), we obtain

$$R = \frac{\sqrt{\pi}}{\omega_0}, \tag{S54a}$$

$$\gamma = \arccos\left(\frac{\omega_0}{\sqrt{\pi}}\right), \tag{S54b}$$

$$\Omega = \omega_0\sqrt{\pi - \omega_0^2}. \tag{S54c}$$

This solution exists for $\pi > \omega_0^2$, i.e., when the fixed points are unstable. This solution corresponds to the one found in Ref. [1], where $\omega_0 = 1$.

5.4 Influence of the bias

The hexbugs used in experiments can be biased, that is they may preferentially turn to the right or to the left. This is due to both fabrication imperfections and intrinsic asymmetry brought by the rotating motor. This bias can be taken into account by adding a constant torque $\tilde{\omega}_B$ in the equation describing the dynamics of the particle polarity. Eq. (S49.3) becomes

$$\dot{\gamma} = \left(\omega_0^2 R - \frac{\pi}{R}\right)\sin(\gamma) + \omega_B, \tag{S55}$$

where $\omega_B = t_0\tilde{\omega}_B$ is the dimensionless bias, with the characteristic time $t_0 = \gamma/k$.

Looking again for orbiting solution, Eq. (S49.1) and Eq. (S49.2) lead to the angular velocity

$$\Omega = \omega_0 \sqrt{\left(\frac{\pi}{R\omega_0}\right)^2 - \omega_0^2}. \tag{S56}$$

and, after substitution, Eq. (S55) reads

$$(\rho - 1)^2 \left(\rho - \frac{\pi}{\omega_0^2}\right) + \frac{\omega_B^2}{\omega_0^4}\rho = 0. \tag{S57}$$

where we have introduced the variable $\rho = R^2\omega_0^2/\pi$, which satisfies the following conditions: by definition $\rho \geq 0$; from the angular velocity $\rho \leq \pi/\omega_0^2$, and assuming that $\sin(\gamma)$ and ω_B are positive implies that $\rho \leq 1$. Only the smallest solution of the last equation satisfies these conditions; the corresponding angular velocity is shown on Fig. S5a.

In Fig 4-c of the main text, we plot the angular velocity as a function of π, and compare it to the result of the above calculation. To do so, one must consider that, experimentally, $\pi = F_0/kl_a$ is varied by changing k (see Methods) and keeping all other experimental parameters constant. Doing so, the characteristic time $t_0 = \gamma/k$ also varies, so that the dimensionless bias ω_B is not constant. To obtain the curve corresponding to the experimental data, one must therefore compute the angular velocity at constant dimensional bias $\tilde{\omega}_B = \omega_B k/\gamma$, namely at constant $\omega_B v_0/\pi l_a$, as illustrated on Fig. S5b.

6 Coarse-grained model

6.1 Continuous fields

Let's remind the microscopic equations written in the main text, and equivalent to Eqs. (S14):

$$\dot{\boldsymbol{u}}_i = \pi\hat{\boldsymbol{n}}_i - \mathbb{M}_{ij}\boldsymbol{u}_j \tag{S58a}$$
$$\dot{\boldsymbol{n}}_i = (\hat{\boldsymbol{n}}_i \times \dot{\boldsymbol{u}}_i) \times \hat{\boldsymbol{n}}_i, \tag{S58b}$$

Now, we want to coarse-grain these equations to be able to describe the continuous limit of active elastic materials. Instead of looking at a discrete elasticity problem, we consider a $2d$ continuous elastic sheet, defined by the deformation field $\boldsymbol{U}(\boldsymbol{r},t)$, and with embedded activity. The orientation of the particles is described by a polarization field $\boldsymbol{m}(\boldsymbol{r},t)$, which can be understood as the mean over the mesoscopic scale of the polarity vectors. Thus we can get rid of the normalization condition the discrete formulation requires, and consider a polarization field with varying amplitude at any point of the sheet, and whose orientation and amplitude are governed by the elastic forces. First we define the average over the mesoscopic scale :

$$\rho(\boldsymbol{r},t)\boldsymbol{m}(\boldsymbol{r},t) = \frac{1}{S}\int_{v(\boldsymbol{r})} \hat{\boldsymbol{n}}(\boldsymbol{r},t)d\boldsymbol{r} = \sum_{i\in v(\boldsymbol{r})} \hat{\boldsymbol{n}}_i(t)\delta(\boldsymbol{r}_i - \boldsymbol{r})$$

$$\boldsymbol{U}(\boldsymbol{r},t) = \frac{1}{S}\int_{v(\boldsymbol{r})} \boldsymbol{u}(\boldsymbol{r},t)d\boldsymbol{r} = \sum_{i\in v(\boldsymbol{r})} \boldsymbol{u}_i(t)\delta(\boldsymbol{r}_i - \boldsymbol{r})$$

where $v(\boldsymbol{r})$ is a disk of small radius, centered at position $\boldsymbol{r}$ and of surface S; and where $\rho(\boldsymbol{r},t)$ is the surface density of active force. Note that for a particle i inside $v(\boldsymbol{r})$, the local fields equal the average value plus the fluctuations, thus $\hat{\boldsymbol{n}}_i(t) = \boldsymbol{m}(\boldsymbol{r},t) + \delta\boldsymbol{m}_i(\boldsymbol{r},t)$ and $\boldsymbol{u}_i(t) = \boldsymbol{U}(\boldsymbol{r},t) + \delta\boldsymbol{U}_i(\boldsymbol{r},t)$, where $\langle\delta\boldsymbol{m}_i(\boldsymbol{r},t)\rangle_{v(\boldsymbol{r})} = \langle\delta\boldsymbol{U}_i(\boldsymbol{r},t)\rangle_{v(\boldsymbol{r})} = 0$. For the rest of this derivation, we consider the density of active force constant in time and space, equal at ρ_0. Moreover, we consider this average density equals to unity, as it simply rescales activity. Within such a framework, the normalization of the polarity vectors, $|\hat{\boldsymbol{n}}_i| = 1$, translates into the constraint $|\boldsymbol{m}(\boldsymbol{r},t)| \leq 1$ for the polarization.

6.2 Strain dynamics

The continuous limit of Eq. (S58a) is simply obtained by averaging over $v(\boldsymbol{r})$, which is trivial as this equation is linear

$$\partial_t \boldsymbol{U}(\boldsymbol{r},t) = \pi\boldsymbol{m} + \frac{1}{S}\int_{v(\boldsymbol{r})} \boldsymbol{f_{el}}(\boldsymbol{r},t)d\boldsymbol{r} \tag{S59}$$
$$\partial_t \boldsymbol{U}(\boldsymbol{r},t) = \pi\boldsymbol{m}(\boldsymbol{r},t) + \boldsymbol{F_{el}}(\boldsymbol{r},t) \tag{S60}$$

where, assuming the average over the local elastic forces leads to the Hooke's law for the continuum elastic force, $\boldsymbol{F}_{el} = \mathrm{div}\sigma = -\mathbb{L}\boldsymbol{U}(\boldsymbol{r}, t)$, with :

$$\sigma = \frac{E}{1+\nu}\left(\varepsilon + \frac{\nu}{1-2\nu}\mathrm{Tr}(\varepsilon)\mathbb{I}\right) \tag{S61}$$

$$\varepsilon = \frac{1}{2}\left(\nabla\boldsymbol{U} + \nabla\boldsymbol{U}^t\right) \tag{S62}$$

where E and ν are respectively the Young modulus and the Poisson ratio of the elastic material.

The displacements field dynamics is composed of a driving term along the polarization field direction, and a relaxation term, which is a second order derivative in space of the displacement field. The elastic term thus smoothes the displacement field on length scales smaller than $l^\star$, obtained from the balance between the two terms:

$$l^\star \simeq 1/\sqrt{\pi} \tag{S63}$$

As a consequence, for a coarse-graining length smaller than $l^\star$, we can safely ignore the fluctuation of the displacement field. This considerably simplifies the coarse-graining of the polarity dynamics.

6.3 Polarity dynamics

Rewriting the dynamics for the polarity Eq. (S58b), using the projector to the normal of $\hat{\boldsymbol{n}}$

$$\dot{\boldsymbol{n}}_i = (\mathbb{I} - \hat{\boldsymbol{n}}_i \otimes \hat{\boldsymbol{n}}_i)\dot{\boldsymbol{u}}_i. \tag{S64}$$

Ignoring the fluctuations of the displacement field, we find:

$$\partial_t\boldsymbol{m} = (\mathbb{I} - \langle\hat{\boldsymbol{n}}_i \otimes \hat{\boldsymbol{n}}_i\rangle)\partial_t\boldsymbol{U}. \tag{S65}$$

Now, we want to express the average $\langle\hat{\boldsymbol{n}}_i \otimes \hat{\boldsymbol{n}}_i\rangle$ as a function of the macroscopic field $\boldsymbol{m}$. By symmetry (in particular, from invariance by rotation), there are only two terms allowed:

$$\langle\hat{\boldsymbol{n}}_i \otimes \hat{\boldsymbol{n}}_i\rangle = \phi(m)\mathbb{I} + \psi(m)\boldsymbol{m}\otimes\boldsymbol{m}, \tag{S66}$$

where $\phi(m)$ and $\psi(m)$ are two functions of m, which must satisfy one additional constraint: since $\mathrm{Tr}(\hat{\boldsymbol{n}}_i \otimes \hat{\boldsymbol{n}}_i) = 1$, one must have for any distribution of orientations:

$$\mathrm{Tr}\langle\hat{\boldsymbol{n}}_i \otimes \hat{\boldsymbol{n}}_i\rangle = 1. \tag{S67}$$

Eventually, the functions $\phi(m)$ and $\psi(m)$ depend on the distribution of the orientations. The limiting cases $m = 0$ and $m = 1$ follow from Eqs (S66) and (S67):

- $m = 0 \Rightarrow \phi(0) = 1/2$ (from Eq. (S67)).
- $m = 1 \Rightarrow \psi(1) = 1$ and $\phi(1) = 0$ (from the equality of all polarity vectors).

As a simple ansatz, we write $\langle\hat{\boldsymbol{n}}_i \otimes \hat{\boldsymbol{n}}_i\rangle$ as the only second order polynomial in m that is compatible with the constraints above:

$$\langle\hat{\boldsymbol{n}}_i \otimes \hat{\boldsymbol{n}}_i\rangle = \frac{1-m^2}{2}\mathbb{I} + \boldsymbol{m}\otimes\boldsymbol{m}, \tag{S68}$$

We finally obtain

$$\mathbb{I} - \langle\hat{\boldsymbol{n}}_i \otimes \hat{\boldsymbol{n}}_i\rangle = \frac{1+m^2}{2}\mathbb{I} - \boldsymbol{m}\otimes\boldsymbol{m} = \frac{1-m^2}{2}\mathbb{I} + m^2(\mathbb{I} - \hat{\boldsymbol{m}}\otimes\hat{\boldsymbol{m}}). \tag{S69}$$

where

$$m^2(\mathbb{I} - \hat{\boldsymbol{m}}\otimes\hat{\boldsymbol{m}})\boldsymbol{A} = (\boldsymbol{m}\times\boldsymbol{A})\times\boldsymbol{m}, \tag{S70}$$

hence

$$\partial_t\boldsymbol{m} = (\boldsymbol{m}\times\partial_t\boldsymbol{U})\times\boldsymbol{m} + \frac{1-m^2}{2}\partial_t\boldsymbol{U} \tag{S71}$$

Altogether, the coarse grained equations read:

$$\partial_t\boldsymbol{U} = \pi\boldsymbol{m} + \boldsymbol{F_{el}} \tag{S72.1}$$

$$\partial_t\boldsymbol{m} = (\boldsymbol{m}\times\boldsymbol{F_{el}})\times\boldsymbol{m} + \frac{1-\boldsymbol{m}^2}{2}\partial_t\boldsymbol{U} \tag{S72.2}$$

6.4 Final form with polarization relaxation

Additionally considering angular noise in the microscopic polarity dynamics (Eq. S14.2), we find that the polarization dynamics (Eq. S72.2) is modified. Let's consider the following microscopic polarity dynamics:

$$\dot{\boldsymbol{n}}_i = \sqrt{2D}\xi_i \hat{\boldsymbol{n}}_i^{\perp} \tag{S73}$$

where ξ_i are i.i.d. gaussian random variables with zero mean and variance $\delta(t-t')$. It is possible to exactly coarse-grain this equation, following the approach of [4]. We find:

$$\partial_t \boldsymbol{m}(\boldsymbol{r},t) = -D\boldsymbol{m}(\boldsymbol{r},t) \tag{S74}$$

Thus the final form for the coarse-grained equations, considering microscopic angular noise:

$$\partial_t \boldsymbol{U} = \pi \boldsymbol{m} + \boldsymbol{F_{el}} \tag{S75.1}$$

$$\partial_t \boldsymbol{m} = (\boldsymbol{m} \times \boldsymbol{F_{el}}) \times \boldsymbol{m} + \frac{1-\boldsymbol{m}^2}{2}\left[\pi\boldsymbol{m} + \boldsymbol{F_{el}}\right] - D_r \boldsymbol{m} \tag{S75.2}$$

where $D_r = D$ is inherited from the particles' angular diffusion coefficient, and contributes to the relaxation of the polarization toward zero.

6.5 Disordered phase

In the absence of the relaxation term ($D_r = 0$), any field $\boldsymbol{m}(\boldsymbol{r},t)$ such that the elastic forces locally balance the activity ($\boldsymbol{F}_{el} = -\pi\boldsymbol{m}$) is a fixed point. However any small amount of noise, microscopic or effectively coming from the coarse-graining procedure, will induce a non zero relaxation term ($D_r > 0$). In that case, any stationary field with $m \neq 0$, relaxes to the only remaining fixed point $\boldsymbol{U} = \boldsymbol{m} = \boldsymbol{0}$.

The linearized equations around this state read:

$$\partial_t \delta\boldsymbol{U} = \pi\delta\boldsymbol{m} + \boldsymbol{F_{el}}\left[\delta\boldsymbol{U}\right] \tag{S76.1}$$

$$\partial_t \delta\boldsymbol{m} = \frac{1}{2}\left(\pi\delta\boldsymbol{m} + \boldsymbol{F_{el}}\left[\delta\boldsymbol{U}\right]\right) - D_r\delta\boldsymbol{m} \tag{S76.2}$$

If $\delta\boldsymbol{U}(\boldsymbol{r},t) = \delta a(t)\boldsymbol{\phi}(\boldsymbol{r})$ and $\delta\boldsymbol{m}(\boldsymbol{r},t) = \delta b(t)\boldsymbol{\phi}(\boldsymbol{r})$, where $\boldsymbol{\phi}$ is an eigenmode of $\boldsymbol{F_{el}}$ such that $\boldsymbol{F_{el}}\left[\boldsymbol{\phi}\right] = -\omega_k^2\boldsymbol{\phi}$, and where δa and δb are small quantities, we get:

$$\frac{d}{dt}\begin{bmatrix}\delta a(t)\\ \delta b(t)\end{bmatrix} = \begin{pmatrix}-\omega_k^2 & \pi\\ -\omega_k^2/2- & \pi/2 - D_r\end{pmatrix}\cdot\begin{bmatrix}\delta a(t)\\ \delta b(t)\end{bmatrix} \tag{S77}$$

Note that expanding $\boldsymbol{\phi}(\boldsymbol{r})$ in the Fourier basis, the eigenfrequencies would be wavenumber-dependent because the elastic force only depends on the gradients of displacement. The solutions λ of the eigenvalue problem satisfy:

$$\lambda^2 - \lambda(\pi/2 - \omega_k^2 - D_r) + D_r\omega_k^2 = 0 \tag{S78}$$

and are represented on Fig. S6.

For $D_r = 0$, one finds two real eigenvalues $\lambda = 0$ and $\lambda = \pi/2 - \omega_k^2$ (Fig. S6a). For $\pi < \min_k(2\omega_k^2) = 2\omega_{\text{min}}^2$, the fixed point is marginally stable. For $\pi > 2\omega_{\text{min}}^2$, it is unstable and the dynamics grow along the lowest energy elastic mode. The coarse-grained description does not contain the non trivial selection observed in discrete systems.

For $D_r > 0$, one finds that the nature of the bifurcation is modified (Fig. S6b). In the relevant small noise regime, the polarization relaxes much slower than the elastic modes $D_r \ll \omega_k^2$ and one finds that:

- when $|\frac{\pi}{2} - \omega_{\text{min}}^2| > 2\sqrt{D_r\omega_{\text{min}}^2}$ (far enough from noiseless threshold), the two eigenvalues are real, with same sign:

$$\lambda = \frac{1}{2}\left(\frac{\pi}{2} - \omega_{\text{min}}^2\right) \pm \frac{1}{2}\sqrt{\left(\frac{\pi}{2} - \omega_{\text{min}}^2\right)^2 - 4D_r\omega_{\text{min}}^2} \tag{S79}$$

- when $|\frac{\pi}{2} - \omega_{\text{min}}^2| < 2\sqrt{D_r\omega_{\text{min}}^2}$ (close enough from noiseless threshold), the two eigenvalues are complex conjugate, with same real part sign:

$$\lambda = \frac{1}{2}\left(\frac{\pi}{2} - \omega_{\text{min}}^2\right) \pm \frac{i}{2}\sqrt{4D_r\omega_{\text{min}}^2 - \left(\frac{\pi}{2} - \omega_{\text{min}}^2\right)^2} \tag{S80}$$

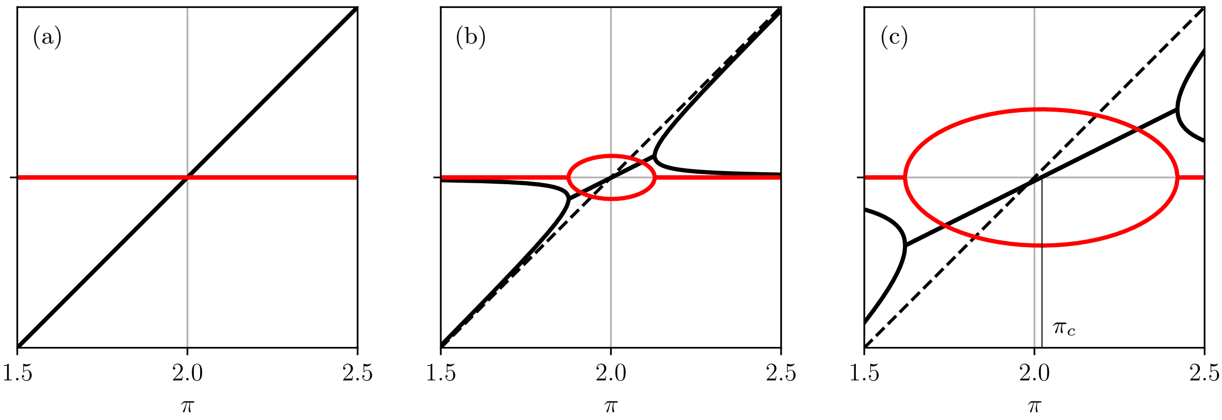

FIG. S6. **Disordered phase instability with long relaxation.** Solutions of Eq. (S78) as a function of the elasto-active feedback π, for $\omega_{\min}^2 = 1$. Black (resp. red) curves represent the real (resp. imaginary) parts of the solutions. (a) $D_r = 0$, (b) $D_r = 10^{-3}$, (c) $D_r = 10^{-2}$.

Thus at threshold $\pi = 2\omega_{\min}^2$, the imaginary part of the eigenvalues writes $\pm i\sqrt{D_r \omega_{\min}^2}$. When $\pi = \pi_c$, the fixed point turns unstable via a Hopf bifurcation

Note that beyond first order in D_r, the instability threshold ($\pi_c = 2\omega_{\min}^2$ in the noiseless case) is shifted to larger values of π : large noise stabilizes the disordered fixed point (Fig. S6c). The oscillation frequency resulting from this Hopf bifurcation is finite at the bifurcation, with an amplitude proportional to $D_r^{1/2}$. It decreases when π is increased further above the instability threshold. With no surprise the linear destabilization properties tell us very little about the disconnected non linear dynamics describing the collective actuation regime.

6.6 Homogeneous phases

We are here interested in describing the physics in the bulk of the material, far from the boundaries, where collective actuation concentrates. In line with the physics of the triangular lattice, let's assume the dynamics condensate on two degenerated modes, which far from the boundaries are homogeneous and akin to the two perpendicular translation modes. By convention, they write: $\langle i|\boldsymbol{\varphi}_1\rangle = \boldsymbol{e}_x$ and $\langle i|\boldsymbol{\varphi}_2\rangle = \boldsymbol{e}_y$.

In this context and neglecting the contributions from all the other modes, the elastic force are homogeneous $\boldsymbol{F}^{el}[\boldsymbol{U}] = -\omega_0^2 \boldsymbol{U}$, where ω_0 is the eigenfrequency of the selected pair of modes. Note that for a fully connected graph of nodes, a mean field realization of the dynamics, the above description is exact, with $\omega_0 = \omega_{\min}$. The coarse-grained equations then read:

$$\partial_t \boldsymbol{U} = \pi \boldsymbol{m} - \omega_0^2 \boldsymbol{U} \tag{S81.1}$$

$$\partial_t \boldsymbol{m} = -\omega_0^2 (\boldsymbol{m} \times \boldsymbol{U}) \times \boldsymbol{m} + \frac{1 - \boldsymbol{m}^2}{2} \partial_t \boldsymbol{U} - D_r \boldsymbol{m} \tag{S81.2}$$

We introduce the angles φ and θ, respectively the angle of the displacement $\boldsymbol{U}$ with respect to the x-axis, and the angle of the polarization $\boldsymbol{m}$ with respect to the x-axis; and the norms R and m of the vectors $\boldsymbol{U}$ and $\boldsymbol{m}$. Once again, we denote $\gamma = \theta - \varphi$. These variables obey the following dynamical equations:

$$\partial_t R = \pi m \cos\gamma - \omega_0^2 R \tag{S82.1}$$

$$R \partial_t \varphi = \pi m \sin\gamma \tag{S82.2}$$

$$m \partial_t \theta = \frac{1 + m^2}{2} \omega_0^2 R \sin\gamma \tag{S82.3}$$

$$m \partial_t m = \frac{1 - m^2}{2} \left[\pi m^2 - \omega_0^2 R m \cos\gamma \right] - D_r m^2 \tag{S82.4}$$

6.6.1 Fixed point

Due to the presence of the relaxation term in Eq. (S82.4), the only fixed point of Eqs. (S82) expresses as ($R_0 = 0$, $m_0 = 0$).

The linearized equations around the fixed point are:

$$\begin{pmatrix} \dot{\delta R} \\ \dot{\delta m} \end{pmatrix} = \begin{pmatrix} -\omega_0^2 & \pi \\ -\omega_0^2/2 & \pi/2 - D_r \end{pmatrix} \begin{pmatrix} \delta R \\ \delta m \end{pmatrix}, \tag{S83}$$

and the eigenvalue problem reduces to solve the polynomial:

$$\lambda^2 - \lambda(\pi/2 - \omega_0^2 - D_r) + D_r\omega_0^2 = 0 \tag{S84}$$

Thus we recover Eq. (S78), with $\omega_{\min}^2 = \omega_0^2$; and the disordered fixed point is stable for $\pi < 2\omega_0^2$, unstable otherwise.

6.6.2 Oscillating solution

Now we look for oscillating solutions of Eqs. (S82) at frequency $\Omega > 0$. It boils down to solve the equation for the amplitude of the polarization:

$$D_r m = \frac{1-m^2}{2} m^2 (\pi - \frac{2\omega_0^2}{1+m^2}) \tag{S85}$$

Without relaxation. If $D_r = 0$, the only solution of Eq. (S85) giving $\Omega > 0$ is $m = 1$. The non-linear saturation vanishes and one recovers the equations for the single particle system, which predict a polarized solution with oscillation at frequency Ω, amplitude R_0 in displacements, and phase shift γ_0 between polarity and velocity vectors, such that:

$$m = 1, \tag{S86.1}$$
$$R_0 = \sqrt{\pi}/\omega_0, \tag{S86.2}$$
$$\cos\gamma_0 = 1/R_0, \tag{S86.3}$$
$$\Omega = \omega_0\sqrt{\pi - \omega_0^2}, \tag{S86.4}$$

when $\pi > \omega_0^2$.

With relaxation. The presence of a small relaxation rate of the polarization amplitude ($D_r = \varepsilon \ll 1$) modifies the picture. Assuming $m = 1 - \delta m$, we find that, for $\pi > \omega_0^2$, $\delta m = \frac{\varepsilon}{\pi - \omega_0^2}$ and

$$m = 1 - \delta m, \tag{S87.1}$$
$$R_0 = \frac{\sqrt{\pi}}{\omega_0}, \tag{S87.2}$$
$$\cos\gamma_0 = \frac{\omega_0}{\sqrt{\pi}}(1 + \frac{1}{2}\delta m), \tag{S87.3}$$
$$\Omega = \omega_0\sqrt{\pi - \omega_0^2}\left[1 - \delta m\left(1 + \frac{1}{2}\frac{\omega_0^2}{\pi - \omega_0^2}\right)\right], \tag{S87.4}$$

As expected, a noisy microscopic dynamics decreases both the polarization and the phase shift γ_0. These two effect balance, resulting in an unmodified value for R_0. The oscillation frequency Ω also decreases with D_r.

7 N particles dynamics : symmetry considerations

Symmetry considerations contribute significantly to the mode selection in two ways. First, together with the normalization condition of the polarization on each mode of the elastic structure, it imposes the selection of some specific modes. Second, it selects the modes which can be nonlinearly actuated, starting from a given pair of modes.

The first step is to sort the modes according to the class of symmetry of the elastic structure of interest, here the triangular and kagome lattices and the linear chain.

7.1 Normal modes sorted by class of symmetry in D_6 geometry

The symmetry group of the triangular and kagome lattices with hexagonal boundaries is the dihedral group D_6. It is generated by the rotation τ of angle $\pi/3$ and a reflection σ (say, of axis $y = 0$), which satisfy $\tau^6 = 1$ and $\sigma^2 = 1$. The eigenvalues of σ are ± 1. The eigenvalues of τ are $\exp(ik\pi/3)$ for $k \in \{-2, \dots 3\}$:

$$\mathrm{Spec}_{D_6}(\tau) = \left(1, e^{i\pi/3}, e^{-i\pi/3}, e^{2i\pi/3}, e^{-2i\pi/3}, -1\right)$$

The eigenmodes associated to the complex eigenvalues are complex and come in pairs: to a mode $|\boldsymbol{\varphi}_+\rangle$ with eigenvalue $e^{in\pi/3}$ is associated a mode $|\boldsymbol{\varphi}_-\rangle$ with eigenvalue $e^{-in\pi/3}$ and with the same energy. These two modes can be combined into two real modes $|\boldsymbol{\varphi}_1\rangle$ and $|\boldsymbol{\varphi}_2\rangle$ with the same energy as $|\boldsymbol{\varphi}_\pm\rangle$. $|\boldsymbol{\varphi}_1\rangle$ and $|\boldsymbol{\varphi}_2\rangle$ are not eigenvectors of τ, but the 2-dimensional space that they span is stable under the action of τ. The action of τ on these modes is characterized by $\langle\boldsymbol{\varphi}_1|\tau|\boldsymbol{\varphi}_1\rangle = \langle\boldsymbol{\varphi}_2|\tau|\boldsymbol{\varphi}_2\rangle$, which is the real part of the eigenvalue of $|\boldsymbol{\varphi}_\pm\rangle$. Hence, the symmetry of a normal mode $|\boldsymbol{\varphi}_k\rangle$ is characterized by two real numbers,

$$\langle\boldsymbol{\varphi}_k|\tau|\boldsymbol{\varphi}_k\rangle \in \{1, 1/2, -1/2, -1\}, \tag{S88.1}$$
$$\langle\boldsymbol{\varphi}_k|\sigma|\boldsymbol{\varphi}_k\rangle \in \{1, -1\}. \tag{S88.2}$$

7.2 Normal modes sorted by class of symmetry in D_2 geometry

The symmetry group of the line is the dihedral group D_2. It is generated by the rotation τ of angle π and a reflection σ (say, of axis $y = 0$). They satisfy $\tau^2 = 1$, $\sigma^2 = 1$. Here, the symmetry of a normal mode $|\boldsymbol{\varphi}_k\rangle$ is thus characterized by two real numbers,

$$\langle\boldsymbol{\varphi}_k|\tau|\boldsymbol{\varphi}_k\rangle \in \{1, -1\}, \tag{S89.1}$$
$$\langle\boldsymbol{\varphi}_k|\sigma|\boldsymbol{\varphi}_k\rangle \in \{1, -1\}. \tag{S89.2}$$

7.3 Symmetry constraint on the mode selection.

The normalization of the polarization, or in other words the fact that the active forces are of constant modulus at every node imposes that the set of activated nodes, as a whole, must contain non zero amplitude displacements on every single node. For instance, in the case of the triangular lattice, the only modes for which the displacement is non zero on the central node are those which are eigenvectors of τ, the rotation in the dihedral group D_6, with eigenvalues $e^{\pm i\pi/3}$. The dynamics must therefore have a finite projection on these modes. This demonstrate that the collective actuation regimes encountered in the triangular lattice pinned at the edges will necessarily include actuations of the $(1/2, \pm 1)$ modes, as indeed observed. Similarly the collective actuation of the line pinned at the edges with an odd number of free nodes includes actuations of the $(-1, \pm 1)$ modes.

The nonlinear couplings then control the transfer of energy between the different symmetry classes. The nonlinearities that are central to the present work, come from the elasto-active feedback. Also they are the only one present in the numerical simulations of the harmonic dynamics. These nonlinearities are best expressed in Eq. (S16.2), which describes the polarity dynamics projected on the normal modes:

$$\frac{da_k^n}{dt} = -\sum_{lpq} \omega_q^2 \Gamma_{pqlk} a_q^u a_l^n a_p^n$$

We see that a mode with eigenvalue λ with respect to the rotation operator can receive energy from modes with eigenvalues λ' only if they satisfy the following relationship $\lambda = \lambda'^3$ (blue squares in Fig. S7). Both in the triangular and kagome lattice cases, the condensed modes, which belong to the symmetry class $(1/2, \pm 1)$ only couple to themselves and to the modes belonging to the symmetry class $(-1, \pm 1)$. This observation explains the precise selection of the secondary peaks in the residual pattern of actuation in Figs. 2-b and 3-e of the main text.

In the experimental system, there are large deformations of the springs for which the harmonic approximation is not valid and nonlinear elastic coupling between the modes also arises. Here also the symmetries restrict the possible couplings : the energy cannot flow from a mode $|\boldsymbol{\varphi}\rangle$ which is symmetric with respect to a symmetry g ($\Gamma_g|\boldsymbol{\varphi}\rangle = |\boldsymbol{\varphi}\rangle$) to a mode which is antisymmetric ($\Gamma_g|\boldsymbol{\varphi}\rangle = -|\boldsymbol{\varphi}\rangle$). On the contrary, the energy can flow from an antisymmetric mode to a symmetric one (black squares in Fig. S7).

8 N particles dynamics restricted to two modes

The strong condensation of the dynamics on a pair of modes cannot be strict, in general, because of the normalization condition of each individual polarity. This is only possible if the two modes $\boldsymbol{\varphi}_1$ and $\boldsymbol{\varphi}_2$ are fully delocalized and locally orthogonal : $|\boldsymbol{\varphi}_k^i| = |\boldsymbol{\varphi}_k^j|$ for every sites i and j and $k \in \{1, 2\}$, and $\boldsymbol{\varphi}_1^i \perp \boldsymbol{\varphi}_2^i$ for every site i. Appart from very specific cases, like the one particle dynamics in the degenerate case studied in the previous section, the pairs of modes of an elastic structure pinned at its boundary do not satisfy such conditions exactly. However, investigating the dynamics restricted to two modes can still provide us with a condition under which a rotating solution sets in.

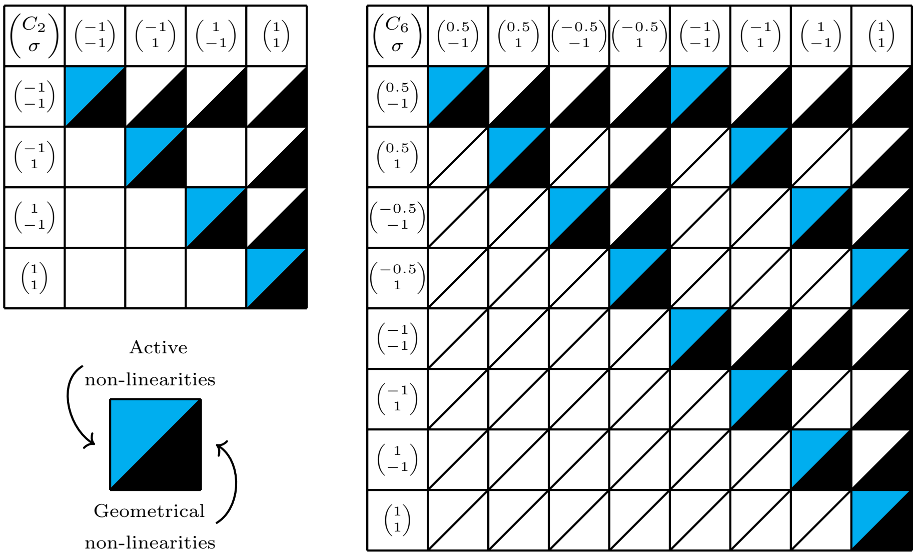

FIG. S7. **Non-linear couplings between symmetry classes.** (left) Inter-class couplings for the dihedral group D_2. (right) Inter-class couplings for the dihedral group D_6. The square (i, j) is colored when energy can flow from the mode of row i to the mode of column j. The upper left blue (resp. lower right black) triangles corresponds to the elasto-active feedback non-linearities (resp. geometrical non-linearities) transferring energy from the class of the row i to the class of the column j.

The dynamics projected on two modes reads:

$$\dot{a}_1^u = \pi a_1^n - \omega_1^2 a_1^u, \tag{S90.1}$$
$$\dot{a}_2^u = \pi a_2^n - \omega_1^2 a_2^u, \tag{S90.2}$$
$$\dot{a}_1^n = -\Gamma_{12}\left(\omega_1^2 a_1^u a_2^n - \omega_2^2 a_2^u a_1^n\right) a_2^n, \tag{S90.3}$$
$$\dot{a}_2^n = \Gamma_{12}\left(\omega_1^2 a_1^u a_2^n - \omega_2^2 a_2^u a_1^n\right) a_1^n, \tag{S90.4}$$

where there is only one coupling constant :

$$\Gamma_{12} = \Gamma_{1212} = -\Gamma_{2112} = -\Gamma_{1221} = \Gamma_{2121} = \sum_i \left(\varphi_1^i \times \varphi_2^i\right)^2 \tag{S91}$$

We note that $a_1^n \dot{a}_1^n + a_2^n \dot{a}_2^n = 0$, hence that the norm $|a^n| = \left({a_1^n}^2 + {a_2^n}^2\right)^{1/2}$ is constant; however, it is not necessarily 1. Introducing the rescaled quantities $\bar{a}_k^n = a_k^n/|a^n|$, where $\bar{a}_k^n$ is now normalized, $\bar{a}_k^u = \Gamma_{12}|a^n|a_k^u$ and $\bar{\omega}_k^2 = \omega_k^2/(\Gamma_{12}|a^n|^2)$, the above equations read

$$\left(\Gamma_{12}|a^n|^2\right)^{-1} \dot{\bar{a}}_1^u = \pi \bar{a}_1^n - \bar{\omega}_1^2 \bar{a}_1^u, \tag{S92.1}$$
$$\left(\Gamma_{12}|a^n|^2\right)^{-1} \dot{\bar{a}}_2^u = \pi \bar{a}_2^n - \bar{\omega}_2^2 \bar{a}_2^u, \tag{S92.2}$$
$$\left(\Gamma_{12}|a^n|^2\right)^{-1} \dot{\bar{a}}_1^n = -\left(\bar{\omega}_1^2 \bar{a}_1^u \bar{a}_2^n - \bar{\omega}_2^2 \bar{a}_2^u a_1^n\right) \bar{a}_2^n, \tag{S92.3}$$
$$\left(\Gamma_{12}|a^n|^2\right)^{-1} \dot{\bar{a}}_2^n = \left(\bar{\omega}_1^2 \bar{a}_1^u \bar{a}_2^n - \bar{\omega}_2^2 \bar{a}_2^u a_1^n\right) \bar{a}_1^n, \tag{S92.4}$$

Up to a rescaling of the time, these are the equations of motion of a particle in an anisotropic potential (Eqs. (S48)). In the degenerate case $\omega_1 = \omega_2 = \omega_0$, rotating solutions exist for

$$\pi > \bar{\omega}_0^2 = \frac{\omega_0^2}{\Gamma_{12}|a^n|^2}. \tag{S93}$$

When the modes 1 and 2 are fully delocalized and locally orthogonal, the condensation can be strict and the restriction to these modes is exact. In this case $\Gamma_{12} = 1/N$ and $|a^n| = \sqrt{N}$ and one recovers the result obtained for one particle in the degenerate case. When these conditions are not satisfied, $|a^n| < \sqrt{N}$ and more modes are activated, which are selected from symmetry considerations as discussed above, in section 6, when considering the geometries specifically studied experimentally. In the numerical simulations of the triangular lattice, we find that $|a_{12}^n| < 0.93\sqrt{N}$.

Altogether, one notes that the higher the scaled condensation level $|a_{12}^n|/\sqrt{N}$ and the stronger the scaled coupling $N\Gamma_{12}$, the lower is the threshold for the existence of a periodic dynamics.

9 Dynamics of linear structures

As we shall see, considering linear structures ensures the existence of pairs of orthogonal modes, hence allowing for further progress in the study of the dynamics.

9.1 Definition of the 1d chain, eigenmodes

We consider a chain with N free particles $1 \leq j \leq N$ and pinned edges $j = 0$ and $j = N+1$. The chain is oriented along $\hat{\boldsymbol{x}}$, so that the equilibrium positions are $x_j = \alpha j$, $y_j = 0$. The parameter α is the the ratio between the length of the springs in the equilibrium configuration l_e and the natural length of the springs l_0; the chain thus bears a dimensionless tension $T = \alpha - 1$.

The dynamical matrix is minus the discrete Laplacian in both directions, with a factor $A_\alpha = 1 - \alpha^{-1}$ in the direction y, and reads

$$\mathbb{M} = \begin{pmatrix} 2 & 0 & -1 & 0 & 0 & 0 & \cdots & 0 \\ 0 & 2A_\alpha & 0 & -A_\alpha & 0 & 0 & & 0 \\ -1 & 0 & 2 & 0 & -1 & 0 & & 0 \\ 0 & -A_\alpha & 0 & 2A_\alpha & 0 & -A_\alpha & & 0 \\ \vdots & & & & & & \ddots & \vdots \\ 0 & 0 & 0 & 0 & \cdots & -A_\alpha & 0 & 2A_\alpha \end{pmatrix}, \tag{S94}$$

where odd (resp. even) lines and columns correspond to displacements along $\hat{\boldsymbol{x}}$ (resp. $\hat{\boldsymbol{y}}$). The directions x and y decouple; as a consequence there are N eigenmodes along $\hat{\boldsymbol{x}}$ (resp. $\hat{\boldsymbol{y}}$), which we denote $\boldsymbol{\varphi}_{x,k}$ (resp. $\boldsymbol{\varphi}_{y,k}$) with eigenfrequencies $\omega_{x,k}$ (resp. $\omega_{y,k}$) :

$$\boldsymbol{\varphi}^j_{x,k} = \sqrt{\frac{2}{N+1}} \sin\left(\frac{jk\pi}{N+1}\right) \hat{\boldsymbol{x}}; \qquad \omega^2_{x,k} = 4 \sin\left(\frac{k\pi}{2(N+1)}\right)^2, \tag{S95.1}$$

$$\boldsymbol{\varphi}^j_{y,k} = \sqrt{\frac{2}{N+1}} \sin\left(\frac{jk\pi}{N+1}\right) \hat{\boldsymbol{y}}; \qquad \omega^2_{y,k} = 4A_\alpha \sin\left(\frac{k\pi}{2(N+1)}\right)^2. \tag{S95.2}$$

The eigenmodes and eigenfrequencies for $N = 2, 3, 4$ and 5 are shown on Fig. S8. The modes in the directions x and y are obviously locally orthogonal. Moreover, modes with the same index k have the same norm on each site, so that we introduce $\varphi^j_k = \boldsymbol{\varphi}^j_{x,k} \cdot \hat{\boldsymbol{x}} = \boldsymbol{\varphi}^j_{y,k} \cdot \hat{\boldsymbol{y}}$. Finally, in the limit $\alpha \to \infty$, which corresponds to infinite tension or zero natural length, $A_\alpha \to 1$ and the modes are degenerated: $\omega_{x,k} = \omega_{y,k} = \omega_k$ for $1 \leq k \leq N$; we restrict ourselves to this case in the following.

9.2 General framework for locally orthogonal and degenerated eigenmodes

9.2.1 Bounds on the stability thresholds

The general bounds derived above (Eqs. (S37) and (S47)) translate into

$$\omega_1^2 \leq \pi_c\left(|\hat{\boldsymbol{n}}^0\rangle\right) \leq 2\omega_1^2. \tag{S96}$$

where the upper bound is obtained with the pair of modes $\boldsymbol{\varphi}_{x,1}$ and $\boldsymbol{\varphi}_{y,1}$.

9.2.2 Single-frequency limit cycles

We look for a collective actuation pattern where all the particles turn with the same constant angular velocity: the orientation $\theta_j(t)$ of the particle j follows

$$\theta_j(t) = \Omega t + \phi_j, \tag{S97}$$

where ϕ_j is a constant phase. Integrating Eq. (S16.1), we deduce that:

$$a^u_{x,k}(t) = a^u_{x,k}(0) e^{-\omega_k^2 t} + \pi \sum_j \int_0^t \varphi^j_k \cos(\theta_j(t-t')) e^{-\omega_k^2 t'} \, \mathrm{d}t' \tag{S98a}$$

$$a^u_{y,k}(t) = a^u_{y,k}(0) e^{-\omega_k^2 t} + \pi \sum_j \int_0^t \varphi^j_k \sin(\theta_j(t-t')) e^{-\omega_k^2 t'} \, \mathrm{d}t' \tag{S98b}$$

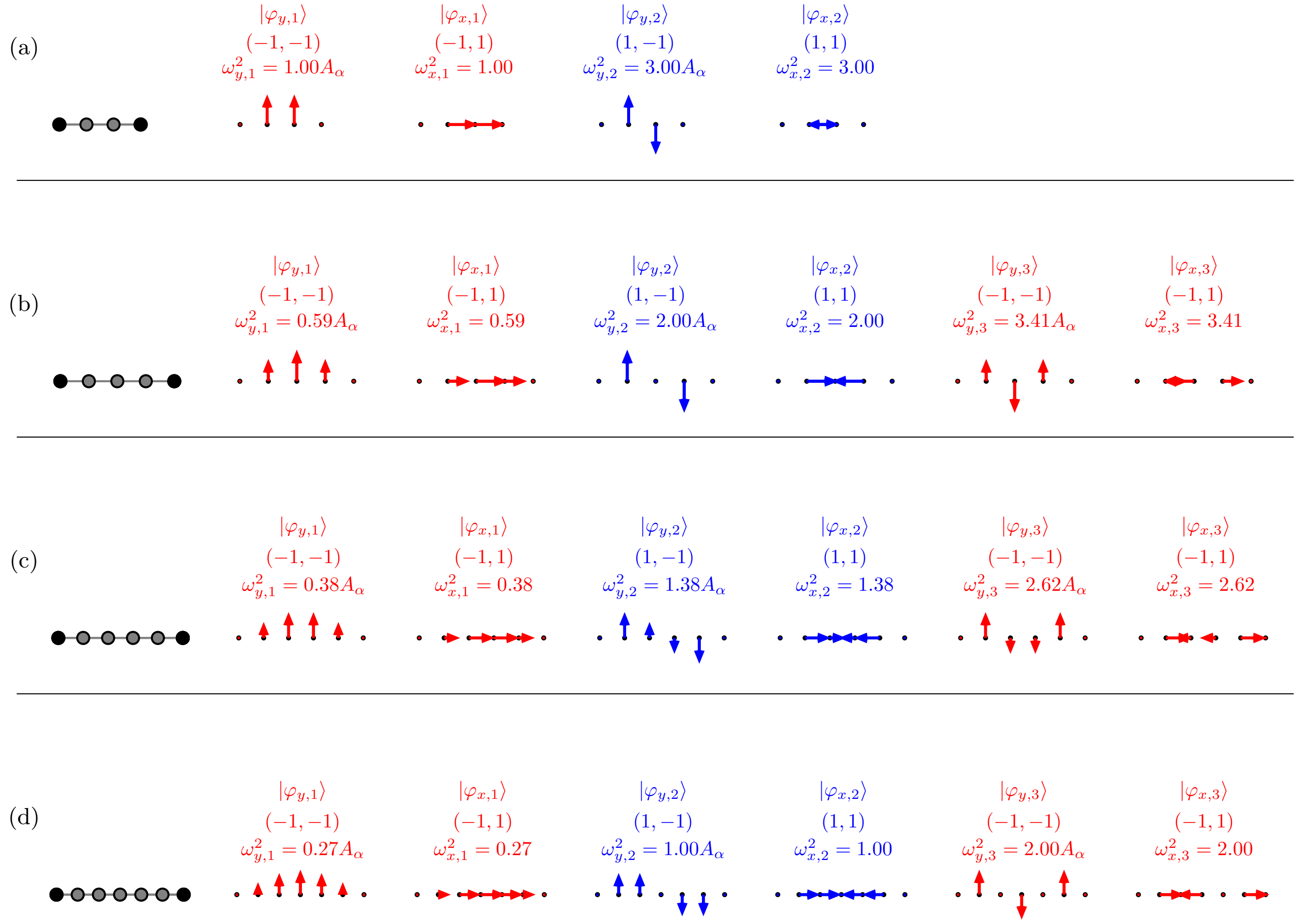

FIG. S8. **Normal modes for linear structures (a) $N = 2$, (b) $N = 3$, (c) $N = 4$, (d) $N = 5$,** sorted by order of growing energies, and colored by their associated eigenvalues with respect to the rotation operation of the dihedral group D_2, characterizing the symmetry of the elastic structure. The modes are computed in the limit of infinite tension, and only the six first modes are shown. For every mode, we show the mode's index k, the eigenvalues associated with the symmetry operations (τ, σ), and the associated squared eigenfrequency ω_k^2.

In the long time limit,

$$a^u_{x,k}(t) = \frac{\pi}{\omega_k^4 + \Omega^2} \sum_j \varphi_k^j f_k(\Omega t + \phi_j), \tag{S99.1}$$

$$a^u_{y,k}(t) = \frac{\pi}{\omega_k^4 + \Omega^2} \sum_j \varphi_k^j f_k\left(\Omega t + \phi_j - \frac{\pi}{2}\right), \tag{S99.2}$$

where we have defined

$$f_k(\theta) = \omega_k^2 \cos(\theta) + \Omega \sin(\theta). \tag{S100}$$

Using the above expressions in the equation for $\dot\theta_j = \Omega$ (Eq. (S13.2)), we get

$$\Omega = \sum_k \omega_k^2 \varphi_k^j \left[\sin(\theta_j) a^u_{x,k} - \cos(\theta_j) a^u_{y,k}\right] = \sum_{k,i} \frac{\pi\omega_k^2}{\omega_k^4 + \Omega^2} \varphi_k^i \varphi_k^j f_k\left(\phi_i - \phi_j + \frac{\pi}{2}\right). \tag{S101}$$

We obtain a set of N equations with N unknowns: Ω and $N-1$ phases (we can always fix one of them). $\Omega = 0$ is always a solution, corresponding to a fixed point. Depending on π, there may be other solutions.

Note that the radii of rotation of the particles can be computed at any time by summing over the modes:

$$R_j = \sqrt{\boldsymbol{u}_j^2} = \sqrt{\sum_{k,l} \varphi_k^j \varphi_l^j (a_{x,k} a_{x,l} + a_{y,k} a_{y,l})}. \tag{S102}$$

9.2.3 Stability of the limit cycles

Each solution may be tested for stability. To determine the stability of a rotating solution, we use the comoving frame and introduce the coefficients β such that:

$$a^u_{x,k}(t) = \beta_{x,k}(t)\cos(\Omega t) - \beta_{y,k}(t)\sin(\Omega t), \tag{S103.1}$$
$$a^u_{y,k}(t) = \beta_{x,k}(t)\sin(\Omega t) + \beta_{y,k}(t)\cos(\Omega t). \tag{S103.2}$$

We now write these coefficients as the rotating solution plus a perturbation:

$$\beta_{x,k}(t) = \beta^{(0)}_{x,k} + \beta^{(1)}_{x,k}(t), \tag{S104.1}$$
$$\beta_{y,k}(t) = \beta^{(0)}_{y,k} + \beta^{(1)}_{y,k}(t), \tag{S104.2}$$
$$\theta_j(t) = \theta^{(0)}_j(t) + \theta^{(1)}_j(t), \tag{S104.3}$$

with

$$\beta^{(0)}_{x,k} = \frac{\pi}{\omega_k^4 + \Omega^2}\sum_j \varphi^j_k f_k(\phi_j), \tag{S105.1}$$
$$\beta^{(0)}_{y,k} = \frac{\pi}{\omega_k^4 + \Omega^2}\sum_j \varphi^j_k f_k\left(\phi_j - \frac{\pi}{2}\right), \tag{S105.2}$$
$$\theta^{(0)}_j = \Omega t + \phi_j. \tag{S105.3}$$

The dynamical equations for these perturbations are derived from (S16.1) and (S13.2):

$$\dot\beta^{(1)}_{x,k} = -\omega_k^2\beta^{(1)}_{x,k} + \Omega\beta^{(1)}_{y,k} - \pi\sum_i \varphi^i_k \sin(\phi_i)\theta^{(1)}_i, \tag{S106.1}$$
$$\dot\beta^{(1)}_{y,k} = -\omega_k^2\beta^{(1)}_{y,k} - \Omega\beta^{(1)}_{x,k} + \pi\sum_i \varphi^i_k \cos(\phi_i)\theta^{(1)}_i, \tag{S106.2}$$
$$\dot\theta^{(1)}_j = \sum_k \omega_k^2\varphi^j_k\left[\sin(\phi_j)\beta^{(1)}_{x,k} - \cos(\phi_j)\beta^{(1)}_{y,k}\right] + \sum_{k,i}\frac{\pi\omega_k^2}{\omega_k^4+\Omega^2}\varphi^i_k\varphi^j_k f_k(\phi_i - \phi_j)\theta^{(1)}_j. \tag{S106.3}$$

9.2.4 Geometrical restriction on the existence of rotating solutions

A simple condition can be derived to determine the stability of the rotating solution found above. Let's remind the equations for a single particle:

$$\dot{\boldsymbol{x}}_i = \pi\hat{\boldsymbol{n}}_i + \boldsymbol{F}^{\mathrm{el}}_i \tag{S107.1}$$
$$\dot\theta_i = \boldsymbol{F}_i\cdot\hat{\boldsymbol{n}}^{\perp}_i \tag{S107.2}$$

where we may express Eq. (S107.2) as:

$$\dot\theta_i = \dot{\boldsymbol{x}}_i\cdot\hat{\boldsymbol{n}}^{\perp}_i \tag{S108}$$

Consider an active particle in the condensed state of the linear chain (i.e. circular motion). From the dynamics periodicity, the angular speed of the position vector and of the polarity vector are the same. Thus:

$$\dot{\boldsymbol{x}}_i = \Omega R_i\hat{\boldsymbol{r}}^{\perp}_i \tag{S109.1}$$
$$\dot\theta_i = \Omega \tag{S109.2}$$

Where R_i is the radius of particle i's trajectory. Then, replacing in Eq (S108), and discarding the $\Omega = 0$ case:

$$\frac{1}{R_i} = \hat{\boldsymbol{r}}^{\perp}_i\cdot\hat{\boldsymbol{n}}^{\perp}_i = \hat{\boldsymbol{r}}_i\cdot\hat{\boldsymbol{n}}_i \le 1 \tag{S110}$$

This means that rotating solutions exist only when the trajectory radius is greater than 1. As π decreases, the radii of rotation of the active units in the rotating solution decrease until the outer-most particles cross the threshold and the rotating solution doesn't exist anymore. In this state, the polarity vector "drifts" with respect to the position of the particle.

9.3 Application to the chain

9.3.1 $N = 2$ chain

The eigenfrequencies are $\omega_1^2 = 1$ and $\omega_2^2 = 3$.

We start by calculating the stability threshold of the fixed points. A fixed point is defined by the orientations θ_1 and θ_2 of the two particles; however, from rotational invariance all the fixed points with the same value of $\Delta\theta = \theta_1 - \theta_2$ are equivalent. Using Eq. (S36), we find their stability threshold, illustrated on Fig. S9:

$$\pi_c(\Delta\theta) = \frac{3}{2 + |\cos(\Delta\theta)|}. \tag{S111}$$

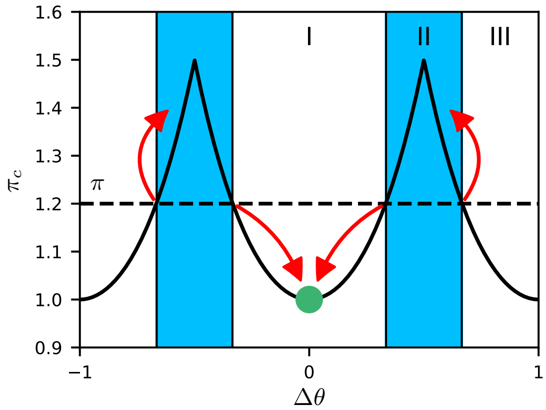

FIG. S9. $N = 2$ **chain: Stability threshold of the fixed points.** The value of π determines which configurations $\Delta\theta$ are stable ($\pi < \pi_c(\Delta\theta)$) and which are not. zone I and III: unstable configurations; zone II: stable configurations. The final configuration reached depends on the initial configuration $\Delta\theta$. All configurations starting in zone I are unstable, and move in phase space up to meet the limit cycle (green dot), corresponding to a condensation on modes $|\boldsymbol{\varphi}_{y,1}\rangle$ and $|\boldsymbol{\varphi}_{x,1}\rangle$. All configurations starting in zone II are stable and thus stay immobile. The red arrows indicate where the corresponding fixed point goes once it destabilizes.

We now look for a rotating solution. Setting $\phi_1 = 0$, the equations (S101) for Ω and ϕ_2 read

$$\Omega = \pi\left[\frac{\Omega(1+\cos(\phi_2)) - \sin(\phi_2)}{2(1+\Omega^2)} + 3\frac{\Omega(1-\cos(\phi_2)) + 3\sin(\phi_2)}{2(9+\Omega^2)}\right] \tag{S112.1}$$

$$= \pi\left[\frac{\Omega(1+\cos(\phi_2)) + \sin(\phi_2)}{2(1+\Omega^2)} + 3\frac{\Omega(1-\cos(\phi_2)) - 3\sin(\phi_2)}{2(9+\Omega^2)}\right] \tag{S112.2}$$

We see that $\phi_2 = 0$ or $\phi_2 = \pi$. For $\phi_2 = 0$ the angular velocity is given by

$$\Omega = \sqrt{\pi - 1}, \tag{S113}$$

which is a valid solution as long as $\pi \geq 1$. To determine the stability of this solution, we need to study the spectrum of the matrix

$$\mathbb{C}_2 = \begin{pmatrix} -1 & \Omega & 0 & 0 & 0 & 0 \\ -\Omega & -1 & 0 & 0 & \frac{\pi}{\sqrt{2}} & \frac{\pi}{\sqrt{2}} \\ 0 & 0 & -3 & \Omega & 0 & 0 \\ 0 & 0 & -\Omega & -3 & \frac{\pi}{\sqrt{2}} & -\frac{\pi}{\sqrt{2}} \\ 0 & -\frac{1}{\sqrt{2}} & 0 & -\frac{3}{\sqrt{2}} & 1 & 0 \\ 0 & -\frac{1}{\sqrt{2}} & 0 & \frac{3}{\sqrt{2}} & 0 & 1 \end{pmatrix} \tag{S114}$$

We are interested in particular in the zero eigenvalues. This matrix always admits one that corresponds to global rotations; it does not preclude the stability of the solution. There is another null eigenvalue when $\pi = 1$, meaning that the rotating solution is stable on its whole range of existence. We can also compute the radius of rotation and obtain $R = \sqrt{\pi}$. This rotating solution is thus very similar to the one of the single particle. Finally, one can show that the rotating solution corresponding to $\phi_2 = \pi$ is unstable.

As a conclusion, for $\pi < 1$ all the fixed points are stable and no rotating solution exists. A rotating solution exists and is stable for $\pi > 1$. For $1 < \pi < 3/2$, the rotating solution coexists with stable fixed points. In this range, starting close to an unstable fixed point, the system either evolves to the limit cycle (for fixed points close to $\Delta\theta = 0$) or to a stable fixed point (for fixed points close to $\Delta\theta = \pi$).

9.3.2 $N = 3$ chain

We restrict our analytical calculations to $\theta_1 = \theta_3 = \theta_2 + \Delta\theta$ and find the stability threshold for the fixed points:

$$\pi_c(\theta_1, \theta_1 - \Delta\theta, \theta_1) = \frac{2}{2 + \sqrt{2}|\cos(\Delta\theta)|}. \tag{S115}$$

The stability threshold ranges from $\pi_c(\Delta\theta = 0[\pi]) = 2 - \sqrt{2}$ to $\pi_c(\Delta\theta = \pm\pi/2) = 1$. We note that $\pi_c(\Delta\theta = 0[\pi]) = \pi_c^{\min} = \omega_{\min}^2$, confirming that these are the most unstable fixed points. On the other hand, we confirm numerically that $\Delta\theta = \pm\pi/2$ correspond to the most stable fixed points.

We turn to the rotating solution. For symmetry reasons, we assume that $\phi_1 = \phi_3$, and we set these phases to 0. From Eq. (S101), we can establish the relation between Ω and π:

$$\frac{4 + 12\Omega^2 + \Omega^4}{2\pi} = 2 + \Omega^2 \pm \frac{8\Omega(\Omega^2 - 2)}{\sqrt{4 + 140\Omega^2 + \Omega^4}}. \tag{S116}$$

Plotting Ω versus π reveals a bifurcation that occurs for $\pi_{CA} \simeq 0.7310$, $\Omega^{CA} \simeq 0.1733$ (Fig. S10): there is no rotating solution for $\pi < \pi_{CA}$, while there are two solutions for $\pi > \pi_{CA}$, a stable one and an unstable one. Contrary to the $N = 2$ chain, the rotation starts with a finite angular velocity Ω_{CA}.

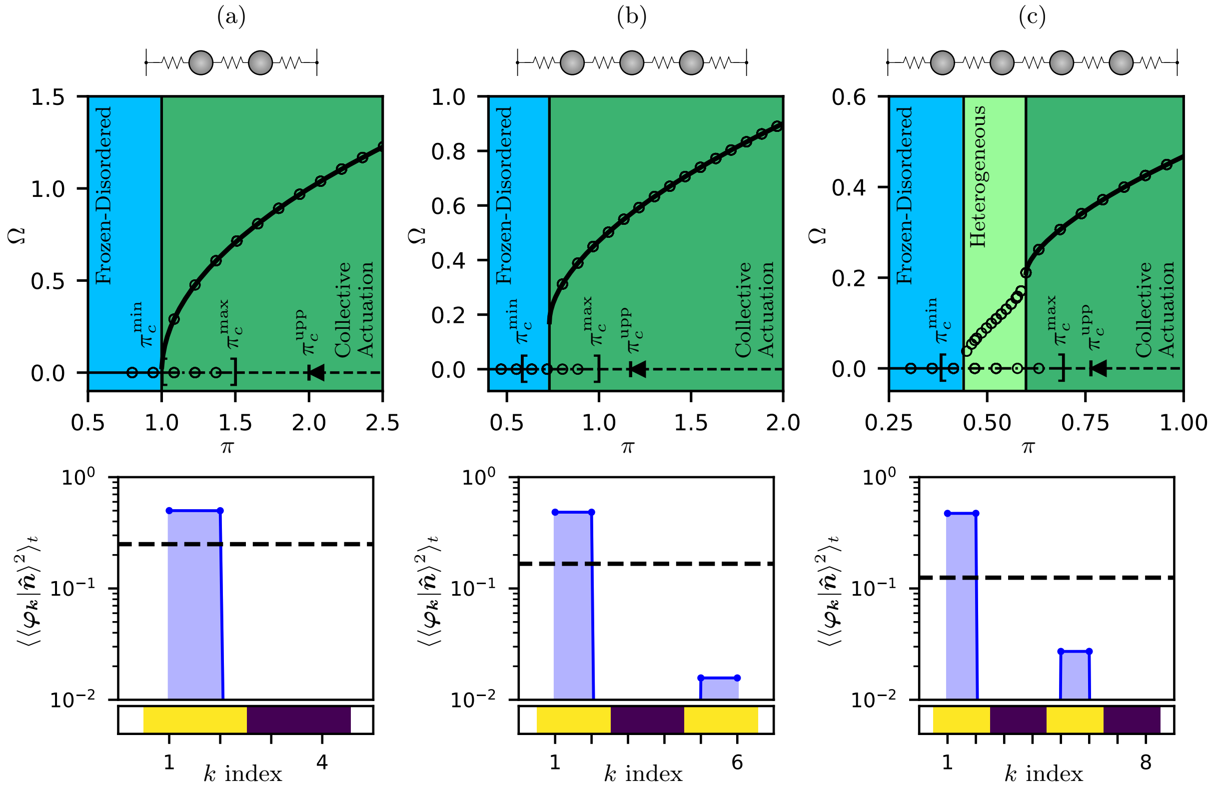

FIG. S10. **Bifurcation of the rotating solution in linear chains.** (a) $N = 2$. (b) $N = 3$. (c) $N = 4$. (top) Bifurcation diagrams of stationary solutions corresponding to single frequency limit cycles. Solid lines represent stable solutions and dashed lines unstable solutions. In (a), $\pi_c^{\min} = 1.0$, $\pi_c^{\max} = 1.5$, $\pi_c^{\text{upp}} = 2.0$, $\pi_{FD} = \pi_{CA} = 1$. In (b), $\pi_c^{\min} = 0.586$, $\pi_c^{\max} = 1.0$, $\pi_c^{\text{upp}} = 1.17$, $\pi_{FD} = \pi_{CA} = 0.731$. In (c), $\pi_c^{\min} = 0.382$, $\pi_c^{\max} = 0.691$, $\pi_c^{\text{upp}} = 0.764$, $\pi_{FD} = 0.440$, $\pi_{CA} = 0.599$. (bottom) Spectral decomposition of simulated collective actuation dynamics (for $\pi = 2.0$) on the normal modes of the different linear structures, sorted by order of growing energies. The horizontal dashed lines indicate equipartition. The bottom color bars codes for the symmetry class of the modes (Supplementary Information section 6).

9.3.3 $N = 4$ chain

The most unstable fixed points destabilize at $\pi_c^{\min} = \omega_{\min}^2 = 4\sin(\pi/10)^2 \simeq 0.3820$. The most stable fixed points are obtained numerically; they destabilize at $\pi_c^{\max} \simeq 0.6908$.

Assuming that $\phi_1 = \phi_4$ and $\phi_2 = \phi_3$, we derive from Eq. (S101) the equation for the rotating solution:

$$\frac{1 + 7\Omega^2 + \Omega^4}{\pi} = \frac{3}{2}(1 + \Omega^2) \pm (1 - \Omega^2)\sqrt{1 - \left(\frac{1 - \Omega^2}{6\Omega}\right)^2}. \tag{S117}$$

The solution presents a bifurcation $\pi_{CA} \simeq 0.5987$, $\Omega_{CA} \simeq 0.2082$.

10 Dynamics of the experimental structures

10.1 Normal modes

Fig. S11 provides the twelve first modes, sorted by class of symmetry, of both experimental structures.

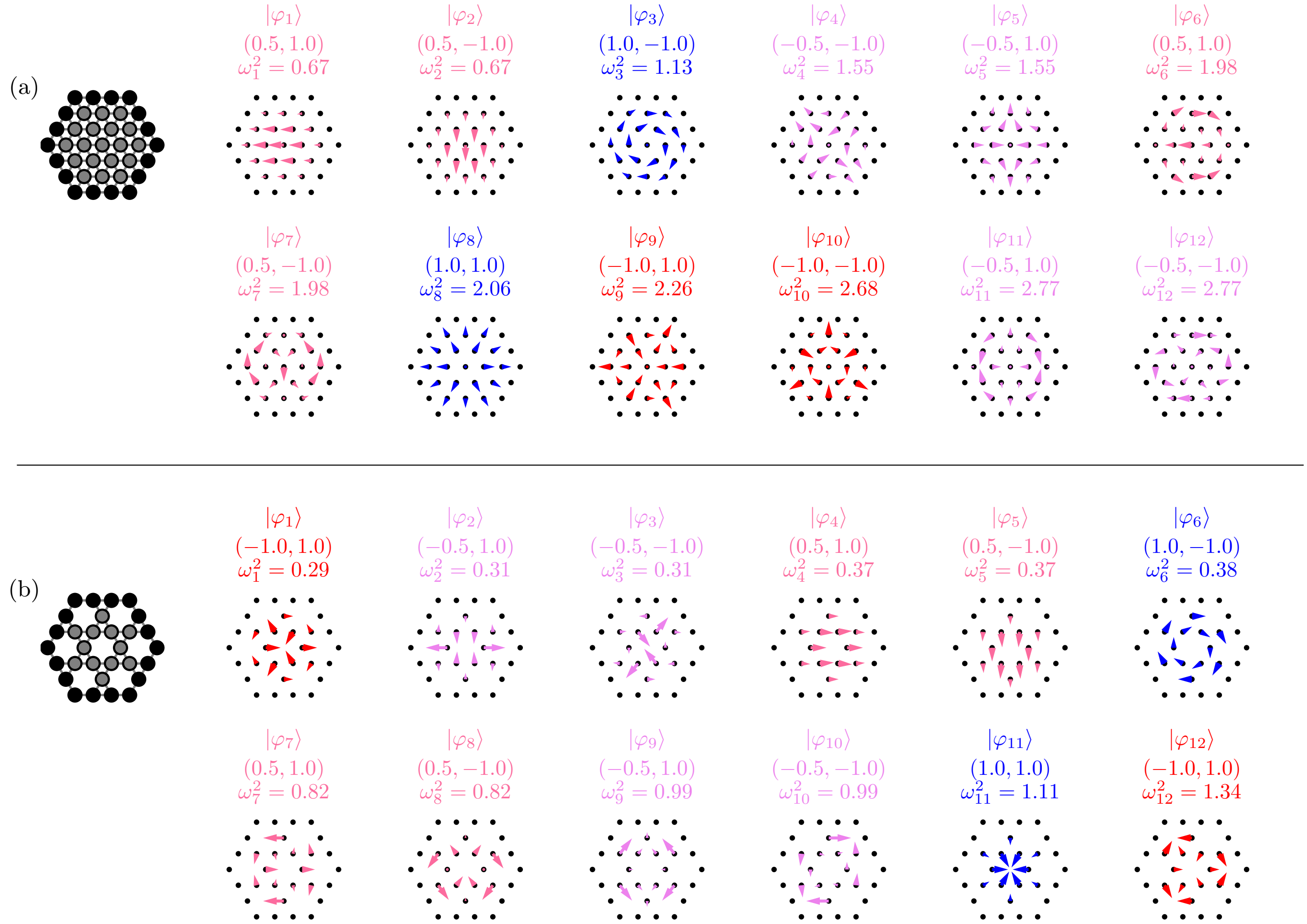

FIG. S11. **Normal modes of the structures studied experimentally: (a) the triangular lattice pinned at the edges (α = 1.27), (b) the kagome lattice pinned at the edges (α = 1.02).** The modes are sorted by order of growing energies, and colored by their associated eigenvalues with respect to the rotation operation of the dihedral group of symmetry D_6 of the structure. The modes are computed for the experimental values of the tension, and only the twelves first modes are shown. For every mode, the figure highlights the mode's index k, the eigenvalues associated with the symmetry operations (τ, σ), and the associated squared eigenfrequency ω_k^2.

10.2 Bifurcation scenarii

From Fig. S11, one sees that the modes concerned by the condensation ($|\boldsymbol{\varphi}_1\rangle$ and $|\boldsymbol{\varphi}_2\rangle$ for the triangular lattice; $|\boldsymbol{\varphi}_4\rangle$ and $|\boldsymbol{\varphi}_5\rangle$ for the kagome lattice) are neither fully delocalized nor locally orthogonal. The D_6 symmetry and the pinning of the nodes at the edges indeed forbid the modes to have such properties. Typically the modes have a larger polarization away from the edges. They are also not strictly locally orthogonal one with another.

The modes $|\boldsymbol{\varphi}_1\rangle$ and $|\boldsymbol{\varphi}_2\rangle$ of the triangular lattice are composed of geometrical domains of nodes, which are equidistant to the central node: (i) the central node (ii) a ring of first neighbors (iii) a ring of second neighbors closest to the center (iv) a ring of second neighbors further away from the center. Similarly, the modes $|\boldsymbol{\varphi}_4\rangle$ and $|\boldsymbol{\varphi}_5\rangle$ of the kagome lattice are composed of domains of nodes equidistant from the center (i) a ring of first neighbors (ii) and a ring of second neighbors.

Fig. S12 describes the details of the noiseless transition from the collective actuation to the frozen regime in the case of the triangular lattice. In the collective actuation regime, the polarities rotate at a given mean frequency, dressed with periodic modulations, (Figs. S12-c,d). Indeed, as the modes concerned by the condensation are not strictly locally orthogonal, the oscillation cannot take place at a single-frequency, and is modulated by even multiples of the mean rotation rate (Fig. S12-e). As π decreases below π_{CA}, the periodic collective actuation regime turns unstable, and the outer domain desynchronize from the mean oscillation. This yields a discontinuous jump in the collective oscillation frequency Ω (Inset of Fig. S12a), and aperiodic turnarounds of the outer domain polarities (Figs. S12f and g). The system has entered into the heterogeneous regime, where the collective actuation and the frozen regimes coexist spatially.

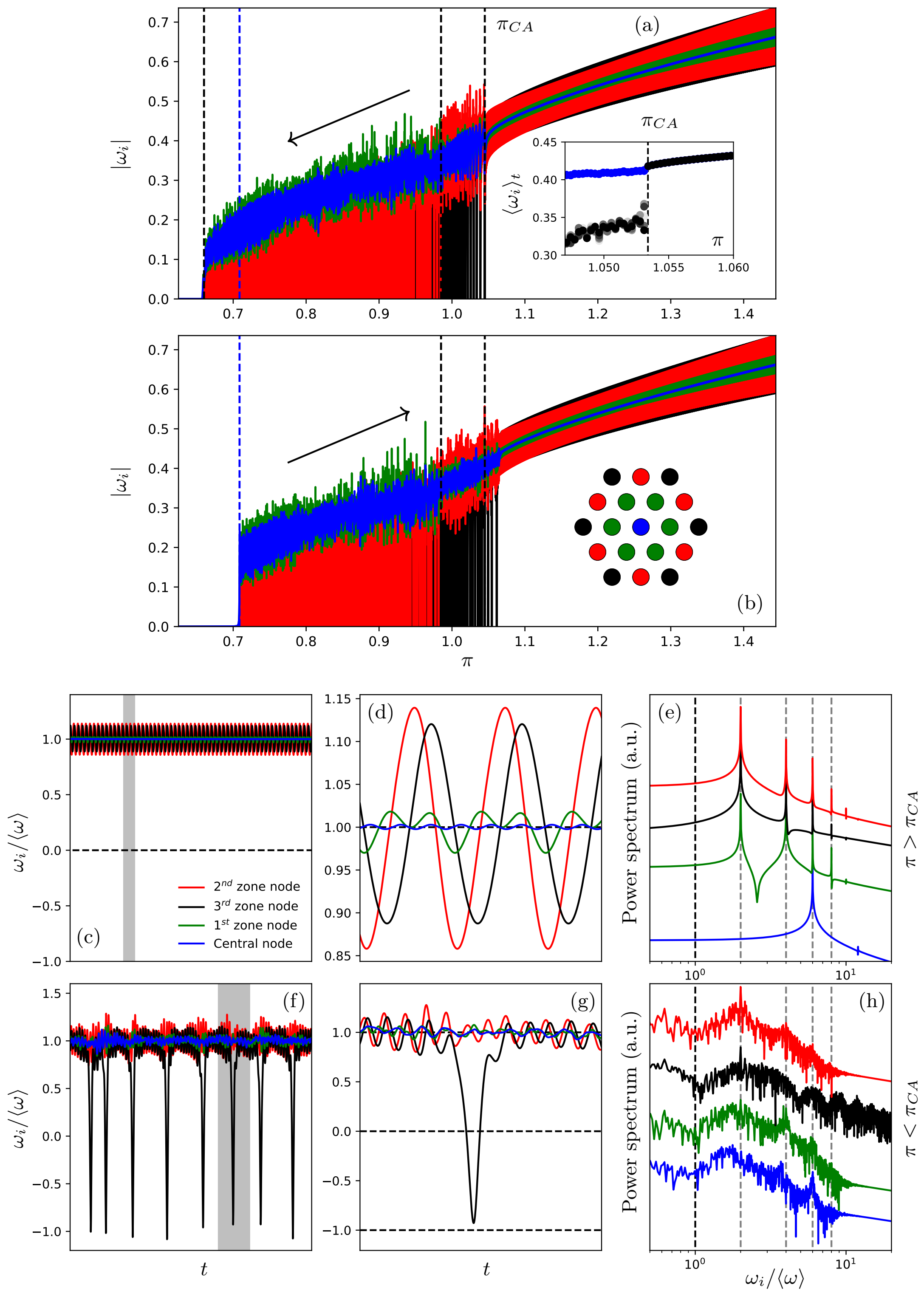

FIG. S12. **Simulations of the bifurcation to the CA condensation in the case of the triangular lattice.** (a) Absolute value of the instantaneous angular velocities $|\omega_i|$ during an annealing experiment with decreasing π. Only four polarities are shown, each representative of a given zone. The black vertical bars show the value of π at which each zone desynchronize. The blue vertical bar highlights the value of π at which the fixed point reached at the end of the process should destabilize (from Eq. (S36)). Inser: time averaged angular velocity for all polarities zoomed on the first desynchronization. The gray level curves represent the 3^{rd} zone polarities. The rest is shown in blue. (b) Inverse annealing process. Inser: definition of the zones. (c/d/e) Dynamics in the physical space just before the first desynchronization; (d) zoom on the gray zone of (c); (e) power spectrums shifted vertically for clarity reasons. (f/g/h) Dynamics in the physical space just after the first desynchronization; (d) zoom on the gray zone of (f); (h) power spectrums shifted vertically for clarity reasons.

References

[1] Dauchot, O., Démery, V. Dynamics of a self-propelled particle in a harmonic trap. *Phys. Rev. Lett.* **122**, 068002, (2018).

[2] Weber, C. A., Hanke, T., Deseigne, J., Léonard, S., Dauchot, O., Frey, E., Chaté, H. Long-Range Ordering of Vibrated Polar Disks. *Phys. Rev. Lett.* **110**, 208001, (2013).

[3] Lam, KDNT., Schindler, M., Dauchot, O. Self-propelled hard disks: implicit alignment and transition to collective motion. *New J. Phys.* **17**, 113056, (2015)

[4] Lam, Khanh-Dang N.-T., Schindler, M. and Dauchot, O. Polar active liquids: a universal classification rooted in nonconservation of momentum. *Journal of Statistical Mechanics: Theory and Experiment* **2015**, 10, P10017, (2015)

[5] Lubensky, T. C., Kane, C. L., Xiaoming Mao, Souslov, A., Kai Sun. Phonons and elasticity in critically coordinated lattices. *Rep. Prog. Phys.* **78**, 073901, (2015).

[6] Alexander, S., Amorphous solids: their structure, lattice dynamics and elasticity. *Physics Reports* **296**, 65-236, (1998).